# Chapter 1
# The Study of Thin Films by Electrochemical Impedance Spectroscopy

**H. Cesiulis, N. Tsyntsaru, A. Ramanavicius and G. Ragoisha**

**Abstract** The capabilities and advantages of electrochemical impedance spectroscopy (EIS) as a useful and non-destructive technique are discussed. EIS provides the time dependent quantitative information about the electrode processes. The description of EIS is given in comprehensive way beginning from the theoretical basics of EIS and data interpretation in the frames of various equivalent electric circuits. The practical applications of EIS are described for the following thin film types: (i) cathodic metals/alloys films deposition; (ii) anodization of metals and characterization of oxide films and its growth by EIS including information provided by Mott-Schottky plots; (iii) underpotential deposition of metals; (iv) characterization of organic films onto metals; (v) application in development of biosensors and biofuel cells. The original data of EIS on cathodic electrodeposition of Co and Co-W are provided and reduction mechanisms involving adsorbed intermediates are discussed. The advantages of EIS in the oxide films characterization and their electrochemical properties are shown. EIS can be successfully applied for the characterization of biosensing surfaces and/or in evaluation of bioanalytical signals generated by biosensors. The glucose oxidase (GOx) based biosensor could be successfully analyzed by merged scanning electrochemical microscopy (SECM) and EIS techniques. Such combining study by SECM and EIS could be very attractive in order to evaluate the biofuel cell efficiency and in the

H. Cesiulis (✉) · N. Tsyntsaru
Department of Physical Chemistry, Faculty of Chemistry, Vilnius University, Vilnius, Lithuania
e-mail: henrikas.cesiulis@chf.vu.lt

N. Tsyntsaru
Institute of Applied Physics, Academy of Sciences of Moldova, Chisinau, Moldova

A. Ramanavicius
Laboratory of Nanobiotechnology, Department of Materials Science and Electronics, Institute of Semiconductor Physics, State Scientific Research Institute Centre for Physical Sciences and Technology, Vilnius, Lithuania

G. Ragoisha
Research Institute for Physical Chemical Problems, Belarusian State University, Minsk, Belarus



I. Tiginyanu et al. (eds.), *Nanostructures and Thin Films for Multifunctional Applications*, NanoScience and Technology,
DOI 10.1007/978-3-319-30198-3_1

modeling of biosensor action, because it is unavailable to obtain by other convenient electrochemical methods.

## 1.1 Introduction

Electrochemical impedance spectroscopy is a recent and powerful tool in corrosion and solid-state laboratories. Electrochemical Impedance Spectroscopy (EIS) also is called AC Impedance or just Impedance Spectroscopy. The usefulness of impedance spectroscopy lies in the ability to distinguish the dielectric and electric properties of individual contributions of components under investigation. Impedance spectroscopy is a non-destructive technique and so can provide time dependent quantitative and time-dependant information about the electrode processes and complex interfaces, extract some characteristics of materials including high resistance materials (e.g. paintings, oxide coatings). There are number of books devoted to the theory, terminology and definitions, and experimental setup of EIS in details, and some of them we recommend for young researchers [1–6]. The aim of this review is to provide information for users about variety of thin films study by EIS in view of general principles of the method.

## 1.2 Basics of EIS

The electrochemical impedance method consists in measuring the response of an electrode to a sinusoidal potential modulation at different frequencies. Often these *ac* modulations are superimposed either onto applied anodic or cathodic potential, or onto open circuit potential. The mathematical approach of electrochemical impedance data is based on the Ohm's law, i.e. on the linear interdependency between potential perturbation and current response or vice versa. However, the potential-current dependencies of electrochemical systems in general are non-linear. On the other hand, it is possible to extract a small fraction of this dependence, where the mentioned dependence can be approximated as linear, e.g. in the range of 5–10 mV. Therefore, the measurements of impedance are performed under sinusoidal potential modulation with amplitude 5–10 mV. The sinusoidal perturbations of potential $E(t)$ induces a sinusoidal current $I(t)$ of the same frequency ($\omega$) superimposed onto the steady state current with the phase shift $\phi$ with the respect to the potential. As for physical electric circuits, the electrochemical impedance of electrode reaction (Z) is defined analogous to Ohm's law as:

$$Z(\omega) = \frac{E(t)}{I(t)} = \frac{|E_0|\sin(\omega t)}{|I_0|\sin(\omega t - \phi)} = Z_0 \frac{\sin(\omega t)}{\sin(\omega t - \phi)} \tag{1.1}$$

here: $E_0$ and $I_0$ is amplitude of potential and current, respectively, $\omega = 2\pi f$ is the radial frequency in rad/s ($f$ is a frequency expressed in Hz).

Here we follow methodology of the description of EIS basic conception provided in [7]. In polar coordinates these functions are represented by vectors of length $|E_0|$ and $|I_0|$ rotating counter clockwise at the radial frequency ω. These functions are most easily described by using complex numbers. With the mathematical identity,

$$\exp(jx) = \cos x + j \sin x \tag{1.2}$$

it is obtained

$$E(t) = |E_0| \exp(j\omega t) \tag{1.3}$$

$$I(t) = |I_0| \exp(j\omega t - j\varphi) \tag{1.4}$$

here $j$ is a complex unit $j = \sqrt{-1}$.

Thus, (1.1) can be rewritten to define the electrochemical impedance as a sum of real ($Z_{\mathrm{Re}}$) and imaginary parts ($Z_{\mathrm{Im}}$) at certain ω:

$$Z(\omega) = |Z_0| \exp(j\phi) = |Z_0|(\cos\varphi + j \sin\varphi) = |Z_0| \cos\varphi + j|Z_0| \sin\varphi = Z_{\mathrm{Re}} + jZ_{\mathrm{Im}} \tag{1.5}$$

Note, that in the electrochemical literature real and imaginary parts of electrochemical impedance often are marked as $Z'$ and $Z''$, respectively.

Using theory of complex functions the modulus of impedance, tanϕ, and ϕ are expressed by a following equations:

$$|Z(\omega)| = \sqrt{Z_{\mathrm{Re}}^2 + Z_{\mathrm{Im}}^2} \tag{1.6}$$

$$\tan\phi = \frac{Z_{\mathrm{Im}}}{Z_{\mathrm{Re}}} \tag{1.7}$$

$$\phi = \arctan\frac{Z_{\mathrm{Im}}}{Z_{\mathrm{Re}}} \tag{1.8}$$

One popular format for evaluating electrochemical impedance data, consists on plotting the imaginary impedance component (Z″) against the real impedance component (Z′) at each excitation frequency the Nyquist plot. This format is also known as a Cole-Cole plot or a complex impedance plane plot. The Nyquist plot has several advantages. The primary one is that the plot format makes it easy to see the effects of the ohmic (uncompensated) resistance (see the text below). If data are taken at sufficiently high frequencies, it is easy to extrapolate the obtained curve toward the left, down to the x axis to read the ohmic resistance. The shape of the curve (often a semicircle) does not change when the ohmic resistance changes.

Another advantage of this plot format is that it emphasizes circuit components that are in series. The Nyquist plot format also has some disadvantages. For example, frequency does not appear explicitly. Secondly, although the ohmic resistance and polarization (charge transfer) resistance can be easily read directly from the Nyquist plot, the electrode capacitance can be calculated only after the frequency information is known.

Another format for evaluating electrochemical impedance data known as Bode plots, and consists of the plotting $|Z(\omega)|$ and $\phi$ versus log$\omega$, i.e. lets to examine these values as a function of frequency. The Bode plot has some distinct advantages over the Nyquist plot. Since frequency appears as one of the axes, it is easy to understand from the plot how the impedance depends on the frequency. The plot uses the logarithm of frequency to allow a very wide frequency range to be plotted on one graph, but with each decade given equal weight. The Bode plot also shows the magnitude ($|Z|$) on a log axis so that you can easily plot wide impedance ranges on the same set of axes. This can be an advantage when the impedance depends strongly on the frequency, as is the case with a capacitor (see text below). The Bode plot is a useful alternative to the Nyquist plot. It lets you avoid the longer measurement times associated with low frequency determinations of polarization resistance, because the log $|Z|$ versus log $\omega$ plot sometimes allows a more effective extrapolation of data from higher frequencies. The Bode plot also has some disadvantages. The greatest one is that the shape of the curves can change if the circuit values change, e.g. uncompensated resistance.

Therefore, usually EIS are analyzed both Nyquist and Bode plots. EIS data is commonly analyzed by fitting it to an equivalent electrical circuit model consisting of passive elements that do not generate current or potential such as resistors ($R$), capacitors ($C$), and inductors ($L$). To be useful, the elements in the model should have a physical meaning in the physical electrochemistry of the system. As an example, most models contain a resistor that models the cell's solution resistance.

The alternating current response of circuit elements are following. A sinusoidal voltage applied to an ohmic resistance induces as alternating current that is in phase with applied voltage, and the impedance of ohmic circuit element is therefore equal to its resistance $R$:

$$Z_r = \frac{E(t)}{I(t)} = \frac{|E_0|\sin(\omega t)}{|I_0|\sin(\omega t)} = R \tag{1.9}$$

Notice that the impedance of a resistor is independent of frequency and has no imaginary component.

The impedance of a capacitor can be calculated based on the relation:

$$I(t) = C\frac{dE(t)}{dt} \tag{1.10}$$

that yields to the expression of capacitance impedance, it's modulus and phase shift:

$$Z_c = -\frac{j}{\omega C} \tag{1.11}$$

$$|Z_c| = \frac{1}{\omega C} \qquad \phi = -\frac{\pi}{2} \tag{1.12}$$

A capacitor's impedance decreases as the frequency is raised. Capacitors also have only an imaginary impedance component. As follows from the detailed derivation of (1.11), the current through a capacitor is phase shifted by 90° with respect to the voltage.

For the inductance, it can be written:

$$E(t) = L\frac{dI(t)}{dt} \tag{1.13}$$

that yields to the expression of inductance impedance, it's modulus and phase shift:

$$Z_l = j\omega L \tag{1.14}$$

$$|Z_l| = \omega L \qquad \phi = \frac{\pi}{2} \tag{1.15}$$

The impedance of an inductor increases as frequency increases. Inductors have only an imaginary impedance component. As a result, the current through an inductor is phase-shifted by −90° with respect to the voltage.

The interpretation of EIS data is built upon reaction model (or equivalent circuit) consisting on passive elements connected in some order. Regardless the variety of electrode processes (deposition and corrosion of metals, electroreduction of ions, oxide film formation, adsorption phenomena, and etc.) they contain the similar stages and comprises similar processes such as formation of double electric layer, the presence of ohmic resistance, charge transfer resistance of electrochemical reaction, adsorbed layers formed by intermediates of complex electrochemical reactions either by protective films, diffusion (transport phenomena) in solutions and in the organic or polymeric films, and etc. Therefore, the same equivalent circuits but with some different physical meaning of passive elements can simulate different processes occurred on the electrode. With the equations of the model it is then possible to calculate the electrochemical impedance as a function of frequency and check conformity experimental data to theoretical model using commercial software, for example ZVIEW® or Autolab® with frequency response analyzer (FRA).

Notably, the reactions occurring consequently are modeling by elements or circuits connected in series, whereas simultaneously occurring processes are modeling by elements or circuits connected in parallel. Mostly used equivalent circuit describing electrode processes are provided in Fig. 1.1. The simplest equivalent circuit can model the electrical behavior of electrode-solution interface is shown in Fig. 1.1a. In this case $R_1$ simulates ohmic resistance (solution, wires and

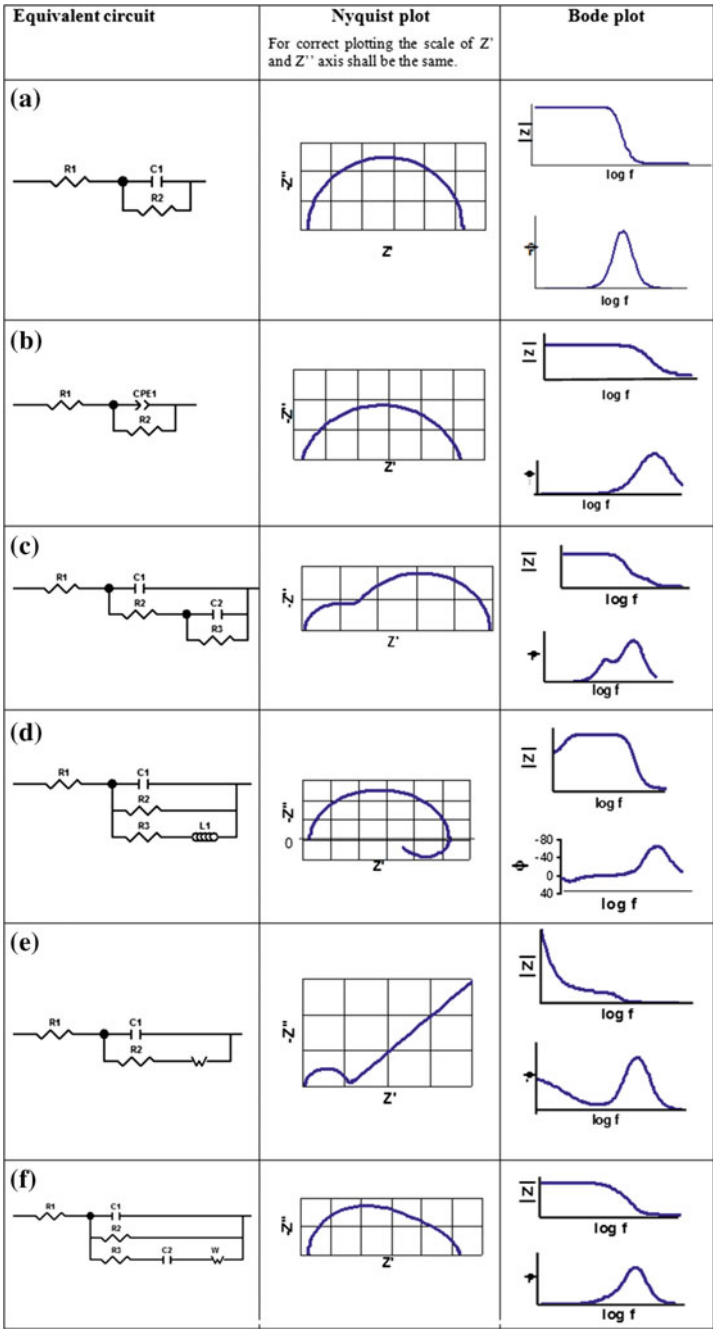


**Fig. 1.1** Often used equivalent circuits to describe electrode processes, typical shapes of Nyquist and Bode plots of ones. For details, see the text

other uncompensated resistances), $C_1$ simulates the capacity of double electric layer which is charged simultaneously with the occurring electrochemical reaction; the charge transfer resistance ($R_p$) of one is simulated by $R_2$. The Nyquist plot represents a semi-circle of radius $R_2/2$ whose center is located on the real axis at the distance $R_1 + ½R_2$ from the origin.

The physical interpretation of the distributed elements in an equivalent circuit modeling solid electrodes is somewhat more complicated than predicted by this model. They are, however, essential in understanding and interpreting most impedance spectra. There are two types of distributions which we need to concern. Both are related, but in different ways, to the finite spatial extension of any real system. The first one is associated directly with nonlocal processes, such as diffusion, which can occur even in a completely homogeneous material, one whose physical properties, such as charge mobilities, are the same everywhere. The other type, exemplified by the constant-phase element (CPE), arises because microscopic material properties are themselves often distributed. For example, the solid electrode–solid electrolyte interface on the microscopic level is not the often presumed smooth and uniform surface. It contains a large number of surface defects such as kinks, jags, and ledges, local charge inhomogeneities, two- and three-phase regions, adsorbed species, and variations in composition and stoichiometry. Reaction resistance and capacitance contributions differ with electrode position and vary over a certain range around a mean, but only their average effects over the entire electrode surface can be observed. The macroscopic impedance, which depends, for example, on the reaction rate distribution across such an interface is measured as an average over the entire electrode [3]. Consequently, in the Nyqist plot the semicircle becomes flattened (Fig. 1.1b). To account for this effect, it has become current practice, especially in corrosion science and engineering, to replace the double layer capacitance (and other capacitances) in the equivalent circuits by a constant phase element (CPE). The impedance of constant CPE is given by:

$$Z(\omega) = \frac{1}{Q}(j\omega)^{-n} \tag{1.16}$$

here $0 < n < 1$, and $Q$ is a constant.

The case $n = 1$ recovers a perfect capacitor.

If electrochemical impedance measurements are performed under reversible potential it is possible to calculate apparent value of exchange current density, $i_0$, and rate of constant of electrochemical reaction, $k_0$ from the charge transfer resistance extracted from the EIS data. If one takes Butler-Volmer equation under the reversible condition, i.e. that in which the overpotential, η, tends to zero, then [8]

$$\frac{\partial i}{\partial \eta} = \frac{1}{R_p} = i_0 \frac{F}{RT} \tag{1.17}$$

The relation of the exchange current density to the rate constant at equilibrium is

$$i_0 = zF\chi k_0 c_i \tag{1.18}$$

here $\chi$ is the thickness of the reaction ion layer

On some electrochemical processes, there is more than one rate-determining step. Each step represents a system impedance component and contributes to the overall reaction rate constant. The electrochemical impedance experiment can often distinguish among these steps and provide information on their respective rates or relaxation times. In such cases, the equivalent circuit contains more elements. For example, if electrochemical reaction involves intermediate stage with one adsorption of reacting intermediate, the equivalent circuit for this case is shown in Fig. 1.1c. The physical meanings for $R_1$, $C_1$, and $R_2$ are the same as in Fig. 1.1a, b. The elements $C_2$ and $R_3$ represent capacitance and resistor of adsorbed layer, respectively. However, this equivalent circuit describes also other processes, such as the presence of non-conductive films (lubricants, paints etc.), therefore passive elements have other physical meanings, and they are noted in the corresponding chapters below.

In fact, the analysis provided in [5] shows that in the simple case of one adsorbed intermediate various complex plane plots may be obtained, depending on the relative values of the system parameters. These plots are described by various equivalent circuits, which are only the electrical representations of the interfacial phenomena. In fact, there are no real capacitances, inductances or resistances in the circuit (faradaic process). These parameters originate from the behavior of the kinetic equations and they are functions of the rate constants, transfer coefficients, potential, diffusion coefficients, concentrations, etc. Besides, all these parameters are highly nonlinear, that is they depend on the electrode potential. It seems that the electrical representation of the faradaic impedance, however useful it may sound, is not necessary in the description of the system. The system may be described in a simpler way directly by the equations describing impedances or admittances.

When transport phenomena play a role, the faradaic impedance can be separated into two terms, the kinetic impedance ($Z_t$) and the diffusion impedance ($Z_d$), and $Z_F = Z_t + Z_d$.

$Z_t$ represents impedance in the absence of concentration overpotential. In some simple cases it can be represented by charge transfer resistance (see Fig. 1.1a), in more complicated cases it may include several circuit elements, e.g. impedance of consequently occurring charge transfer reactions (Fig. 1.1c). $Z_d$ describes the contribution of concentration overpotential to the faradaic impedance, and therefore depends on transport phenomena in the solution. In the absence of convection, it is referred as Warburg impedance $Z_W$. The Warburg impedance is equal to:

$$Z_W = \frac{\sigma}{\sqrt{\omega}} - j\frac{\sigma}{\sqrt{\omega}} \tag{1.19}$$

$$\sigma = \frac{RT}{C_{st} n^2 F^2 A \sqrt{2D}}$$

As follows from (1.19):

$$\tan \phi = \frac{Z_{\mathrm{Im}}}{Z_{\mathrm{Re}}} = -1 \tag{1.20}$$

Therefore, the phase shift is equal to $\phi = -45°$, and in the Nyquist plot the Warburg impedance is represented by a straight line at 45° angle. If charge transfer is represented only by one resistance ($R_p$ = R2), the total impedance of the electrode corresponds to that of the Randles equivalent circuit, as it is shown in Fig. 1.1e. In this figure Nyquist diagram consists of two distinct domains: at high frequency, a semicircle shows that the transfer resistance determines the impedance, while at low frequencies diffusion dominates and Warburg impedance is observed. However, in some cases, the kinetics of electrode processes is more complicated [9], because of the adsorption of intermediates and components of solutions (e.g. ligands) coupled with charge transfer and diffusion processes. Therefore, it is impossible to distinguish frequencies ranges at those the kinetics or mass transfer controls electrode processes based on the experimental EIS data (some of these were published for ex. in [10, 11]).

Analysis of the ac impedance spectra in the presence of specific adsorption revealed that the complex plane show formation of deformed semicircles, that might be described by introducing into equivalent circuit CPE. Authors [12] proposed an electrical equivalent model, in which instead of the CPE there is a double-layer capacitance in parallel with a series connection of the adsorption resistance and capacitance, $R_{ad}$ and $C_{ad}$ (R3 and C2 in Fig. 1.1f), and the semi-infinite Warburg impedance (W) connected with the diffusion of adsorbing species. This equivalent circuit allows describing various shapes of Nyquist plots, such as 2 semicircles, depressed one semicircle, and other.

Other more specific equivalent circuits are provided in the corresponding chapters of this paper below.

The impedance technique is often applied to various electrochemical systems that were never studied before. The Nyquist and Bode plots obtained often display shapes that had never been encountered previously. Before starting the analysis and modeling of the experimental results, it should be confirmed that the impedance data are valid. There is a general mathematical procedure, which allows for the verification of the impedance data. It was introduced by Kramers in 1929 and Kronig, 1926 further developed by Bode in 1945 and later applied to EIS [13]. The impedance derived is valid provided that the following four criteria are met: (i) linearity (a system is linear when its response to a sum of individual input signals is equal to the sum of the individual responses); (ii) causality (the response of the system must be entirely determined by the applied perturbation, that is the output depends only on the present and past input values); (iii) stability (a stable system remains stable unless excited by an external source and it should return to its original state once the perturbation is removed and the system cannot supply power to the output irrespective of the input); and (iv) finiteness (the real and imaginary components of the impedance must be finite-valued over the entire frequency range

$0 < \omega < \infty$, i.e. the impedance must tend to a constant real value for $\omega \rightarrow 0$ and $\omega \rightarrow \infty$. Unfortunately, the Kramers-Kronig transform requires integration over a range of frequency from zero to infinity. Since no one can measure spectral data over that range, evaluating the K-K relations via integration always involves assumptions about the behavior of a spectrum outside the frequency over which it was measured. The transformation procedure is described in details in for ex. [3–5, 13]. In practice, the Kramer-Kronig transformation is possible to perform using built in the EIS recording devices corresponding software, e.g. Gamry Echem Analyst or Autolab® with FRA. When you select Kramers- Kronig on an impedance menu a model of the type is fit to the selected region of the spectrum. If the fit is poor, you can assume that the data is not transformable and is therefore of poor quality. There is little point fitting non-Kramers-Kroning compliant data to an equivalent circuit model.

## 1.3 EIS Responses During Cathodic Metals and Alloys Films Deposition

Electrochemical impedance spectroscopy (EIS) responses during electrodeposition have gained the interest last decades due to possibility to determine several parameters of the systems e.g. double-layer capacitance, to characterize the electrode processes and to determine the kinetics of the electrochemical systems. The use of this technique in metals/alloys electrodeposition in the presence of complexes or additives has also high impact since adsorption phenomena strongly influence the electrochemical impedance [14–18]. One of its advantages is the possibility of investigation the relaxation of the electrode surface from adsorbed species and growth of layers. The impedance spectra of the deposition processes of metals/alloys usually show one or several relaxations (capacitive or inductive) [19, 20]. Thus, using electrochemical impedance spectroscopy, the electrodeposition of Co and Co-W were studied by authors in order to compare the differences of the deposition and codeposition of Co with tungsten and the effect of the pH on these processes.

The cobalt and cobalt alloys are investigated for their magnetic and corrosion resistant properties by many groups of researchers, including [21]. The interest in tungsten and its alloys has been driven by its outstanding properties and multiple possible applications overviewed by E. Lassner and W.D. Schubert [22] and recently by N. Tsyntsaru and others [9]. The first commercial Co-W alloy electrodeposition process was reported by Schwartz [23], indicating the role of citrate species as an important factor to achieve the desirable morphology and structure of deposits. Complexing is used as a method to approach the electrode potentials of different metals by reducing the concentration of "free" $Me^{2+}$" ions and increasing the solubility of Me(II) salts in baths containing $OH^-$, $WO_4^{2-}$ and $PO_4^{3-}$ [24, 25]. Several common electrolytes are known and used for the electrodeposition of

tungsten alloys with iron-group metals but the number of complexing agents used is limited (citrates, pyrophosphates [26, 27], tartarates [28, 29], gluconates [30, 31]). The presence in such electrolytes the species with high molecular weight [32, 33] is the particular feature of the given systems which influence the mechanism of electrodeposition.

However, some difficulties to describe the mechanism and kinetics of tungsten codeposition with iron group metals (Fe, Co, Ni) are related with rare data about the mechanism and kinetics of pure iron group metal complexes electroreduction and identification of the electrochemically active complex of metal that participates in the electrochemical charge transfer reaction in complex solutions. Even in the "simple" case of cobalt electrodeposition, the process actually is complex and multistaged, caused by transfer of two electrons for cobalt reduction to metal state and by the parallel process of hydrogen evolution. This secondary process increases the pH of the near-electrode layer and induced the formation of $CoOH^+$ on electrode surface [34], effect on the kinetics and mechanism of cobalt electrodeposition [35–38].

As an example, data on Co electrodeposition from various solutions are discussed below. The polarization curves at the same total Co(II) concentration in the electrolyte are presented in Fig. 1.2. The differences are caused by the different ionic content of solution due to the formation of ionic pairs (sulphate electrolyte) and complexes (citrate electrolyte). However, from the first view, the shape of these curves is similar to the shapes obtained for the processes of mixed kinetics (charge transfer and diffusion). In this case the plateau evident on the curves should be linked to limiting diffusion current. On the other hand, it is not expected such big differences in diffusion coefficients of various Co(II) compounds. Moreover, if this plateau is linked to limiting diffusion current, in accordance with equation describing the Warburg impedance $Z_W$ shall be equal to infinity when concentration at the electrode surface ($c_{st,s}$) becomes equal to zero in according to (1.19).

Therefore, the whole impedance of electrode process shall become infinitive too.

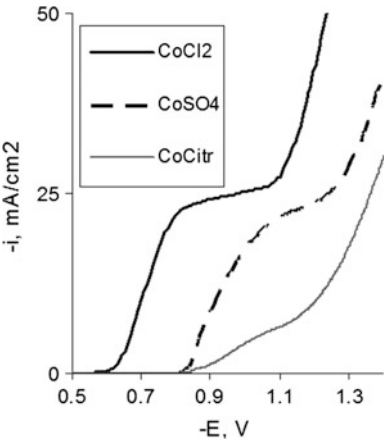


**Fig. 1.2** Polarization of Co electrode in the various electrolytes: chlodide: 0,25 mol/l $CoCl_2$ + 0.4 mol/l NaCl + 0.25 mol/l $H_3BO_3$ pH 6; sulphate: 0.25 mol/l $CoSO_4$ + 0.5 mol/l $Na_2SO_4$ + 0.65 mol/l $H_3BO_3$ pH 6; citrate: 0.25 mol/l $CoCl_2$ + 0.4 mol/l $H_3BO_3$ + 0.4 mol/l $Na_3C_6H_5O_7$ pH 6

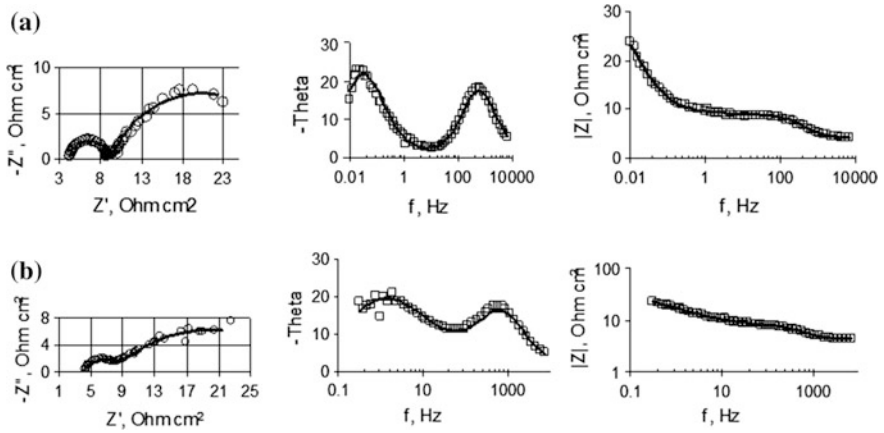


**Fig. 1.3** EIS (Nyquist and Bode plots) obtained in the sulphate solution (content as in Fig. 1.2) on Co and fitting results to the equivalent circuit (Fig. 1.1c) at the potentials: **a** E = −1.00 V, **b** E = −1.20 V

The EIS data obtained in the sulphate electrolyte on Co at the "plateau" potentials presented in Fig. 1.3 show relatively small values of real and imaginary parts and spectra fit well to the equivalent circuit containing elements simulating stage of intermediate adsorbed compound (Fig. 1.1c), probably of $CoOH^+$, similarly to the case of Ni and Fe electrodeposition [39, 40]. Also, the analogous EIS data were obtained in [41] for the cases of Ni electrodeposition from chloride, sulphate and citrate solutions. In addition, this point of view is confirmed by EIS data obtained also in citrate solutions for Co-Cu alloys electrodeposition [42], where was shown that the reduction of Cu(II)-citrate and Co(II)-citrate is divided into two steps. The Cu(II)-citrate and Co(II)-citrate are first reduced to an intermediate state and then to $Cu^0$ and $Co^0$. Adsorption exists at the surface of the electrode at the potential of about −1.0 V.

The polarization curve for Co-W electrodeposition and corrected for ohmic drop are shown in Fig. 1.4. It is similar as for the processes with the ionic mass transfer determining step.

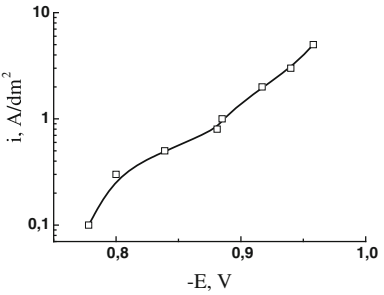


**Fig. 1.4** Polarization curves of Co-W electrodeposition obtained under natural convection and subtracted of ohmic drop

The results obtained by us [10] suggest that the process under study is more complex than the classical process of mixed kinetics (slow charge transfer plus slow convective diffusion). The first complexity lies in the fact that, due to the complex formation at pH > 4, the concentration of the electroactive particles significantly differs from the analytical value; hence, the respective diffusion currents and the diffusion coefficients that are determined on their basis decrease. The second complexity is due to the possibility of the formation of intermediates (in the bulk solution or on the electrode surface) and their reduction is a multistage process that includes intermediate adsorption and interaction in the adsorption stage. One of the methods for determining the role of the ionic mass transfer (the diffusion in the solution) in this process can be electrochemical impedance spectroscopy, which was applied by us.

The data presented in Fig. 1.5 show that the shape of the impedance spectra does not imply a slow diffusion stage. The presence of two peaks in the Bode diagram excludes a single slow stage of charge transfer. Also note that, if in the case of the deposition of Co-W at pH = 6.7 at low cathode potentials the electrochemical impedance spectrum is described without separate adsorption component (Fig. 1.5a), then an increase in the potential leads to an increase in the hydrogen evolution and hence in the alkalization of the near electrode layer, which results in the appearance of an adsorption component at potentials above –0.7 V (Fig. 1.5b).

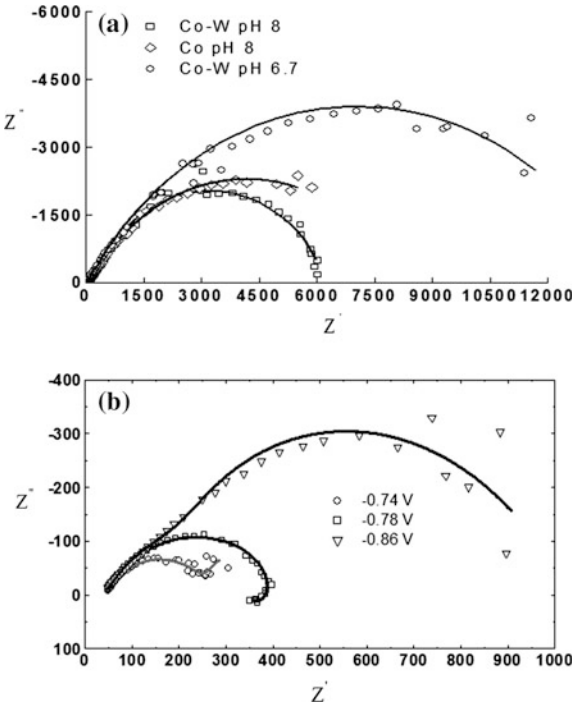


**Fig. 1.5** Comparison of the experimental electrochemical impedance spectra for Co and Co-W obtained from citrate electrolytes and the results of fitting in Nyquist and Bode coordinates to the equivalent circuit shown in Fig. 1.1c

Meanwhile, at a higher value of the pH (equal to 1.8), electrochemical impedance spectrum is described by the equivalent circuit with separate adsorption at low and high cathode potentials. The presence of an adsorption complex at high pH values also plays a fundamental role in the deposition of a simpler system, such as the electrodeposition of cobalt (Fig. 1.5a).

Thus, these experimental data are adequately described by an equivalent electric circuit characteristic of the processes that include the adsorption of an intermediate compound, the double layer capacity and the adsorption capacity are replaced by the respective constant phase elements. Applied to the electrodeposition of iron group metals with tungsten/molybdenum the following sequence of reactions can be attributed to this process:

$$\mathrm{M(II)L} + e^- \rightarrow \mathrm{M(I)L_{ads}} \tag{1.21}$$

$$\mathrm{M(I)L_{ads}} + e^- \rightarrow \mathrm{M(s)} + \mathrm{L} \tag{1.22}$$

$$\mathrm{WO_4^{2-}} + \mathrm{M(II)L} + 2\mathrm{H_2O} + 2e^- \rightarrow \mathrm{[M(II)LWO_2]_{ads}} + 4\mathrm{OH^-} \tag{1.23}$$

$$\mathrm{[M(II)LWO_2]_{ads}} + 2\mathrm{H_2O} + 4e^- \rightarrow \mathrm{W(s)} + \mathrm{M(II)L} + 4\mathrm{OH^-} \tag{1.24}$$

Thus, the equivalent circuit shown in Fig. 1.1c is not the only one describing the impedance spectrum of a process with the adsorption of an intermediate compound. Depending on the ratio of the rates of the reactions of the total process (1.21–1.24), which also depend on the potential, a situation can occur when the resulting phase shift will correspond to the inductance; that is, so called pseudoinductance will take place and is modelled by equivalent circuit shown in Fig. 1.1d. In this case the inductance simulates the situation when the adsorption layer is not constant under cyclic changes in the low frequency potential [43]. The similar equivalent circuits are also obtained in [40].

Thus, the data of the impedance measurements show the presence of adsorption processes in the systems under study and the impedance does not specify the chemical composition of the adsorbed layer or the number of adsorption stages. It only shows the presence of a slow adsorption stage that follows from the data. Regardless of the complexes used for the codeposition of Co and W (individual or mixed cobalt–tungsten), the reduction of Co(II) and W(VI) requires a certain number of electrons (two for cobalt and six for tungsten). The simultaneous transfer of this number of electrons is hardly probable; therefore, a partially reduced complex is apparently held on the surface, in particular, by adsorption forces. The data for the impedance also suggest that the stirring of the electrolyte has an effect on the state of its surface rather than on the mass transfer from the solution to the electrode. It follows from the results of [44] that, at pH ≤ 4, the electrochemically active particles are an aquatic complex of $Co^{2+}$; therefore, the calculated value of the diffusion coefficient is “unsual” in this case.

At higher pH values, the electrochemically active particles will be both cobalt hydroxocomplexes [40, 43] and citrate complexes of cobalt as well as (possibly)

mixed cobalt–tungsten citrate complexes. As the pH increases, their concentration changes and the adsorbed citrate complexes undergo a structuring. It is also known (see, e.g., [45]) that the concentration of the cobalt aquatic complexes in the solution and the current density of the electrodeposition decrease at pH > 5. The hydrogen evolution on the electrode favors a local increase in the pH. With the rotation of the electrode, the local increase in the pH sharply slows down, which leads to a decrease in the concentration of the adsorbed complexes and an increase in the electrodeposition current's density. In a galvanostatic mode, at a constant current density, this results in an increase in the current efficiency; a lowering of the electrodeposition potential; and a decrease in the concentration of tungsten in the coating [46], which, in turn, is one of the causes of changes in its structure [47] and hence properties [48].

## 1.4 Anodization of Metals: Characterization of Oxide Films and Their Growth by EIS

Anodization, because of its nature-friendly properties and low cost, has become a point of interest in the last century. Anodizing is an electrochemical process which is performed to form a protective oxide layer on the surface of a metal. Other methods such as evaporation or plasma enhanced chemical vapor deposition (PECVD) are known to be used also for oxidation. But among these, advantages of anodizing make it more attractive. Low cost, more precise thickness control and easier handling of process can be given as examples to these advantages [49]. Anodization can be used in different fields or for different applications. Protection of a surface against corrosion, decorative metal finish, architectural and nanotechnology applications, electrolytic capacitors, humidity sensors, self-lubricating systems and aerospace structures can be given as examples [50–53].

Anodic film formation of various thickness and structure is mostly applied on titanium (Ti) and aluminium (Al). However, zinc, magnesium, niobium, tantalum and iron can also be anodized [52]. For valve metals such as Al, Ti, Ta, or Zr, anodization has been extensively explored and, by a controlled variation of the electrochemical parameters used, the thickness, morphology e.g., compact or porous layers or crystal structure of the anodic films can be tailored to achieve the desired functionality [54]. Either a thick non-porous oxide or a film consisting of pores in nano-scale can be achieved by anodizing [49].

The porous structure of the anodic layers provides the oxides with absorbent characteristics which increase their applications. Nevertheless, in those applications where the oxides are atmospherically exposed, sealing of the anodic layers is required because porosity decreases the corrosion resistance [55]. The sealing process achieves an important reduction in the porosity of the anodic layer. Atmospheric exposure of the oxide produces significant changes in the anodic layer (due to the autosealing process) increasing the material corrosion resistance

[56, 57]. The corrosion resistance depends on layer thickness and especially on the sealing quality, so good quality control on both parameters has maximum significance. There are many different experimental evaluation techniques which offer interesting information, but all of them have their limitations [57]. The application of electrochemical impedance spectroscopy to the oxide films characterization has many advantages. The results show that EIS is a powerful tool able to provide tiny pieces of information on the films electrochemical properties, and not least in which way atmospheric exposure can modify the anodized samples properties [57–61]. Hoar and Wood [62] were first proposing an impedance bridge to describe oxide films; they suggested ECs to model unsealed and partially sealed anodized films [55]. Lorenz and other authors proposed the "passive pit model" (where it is assumed that pits have penetrated only the outer porous layer without damaging the barrier layer) and the active pit model (where it is assumed that pits have penetrated both the porous and barrier layer) [60, 61, 63, 64]. As pointed out by Mansfeld and Kendig [60], the passive pit model can also be used to interpret the sealing mechanism.

Electrochemical impedance spectroscopy has been used to characterize oxide films on titanium surface [65–71]. Thus, in [71] the surface treatment consisted of an etching followed by an anodising procedure of titanium and sample sealing. Anodic oxide films were grown electrochemically on titanium surface using modulated potential, in hydrofluoric acid solution aiming for the production of a porous film. It is assumed that the oxide film is a two-layer film, consisting of one inner barrier layer and an outer porous layer The effect of surface etching before anodising, oxide film sealing is analyzed using the equivalent electrical circuit proposed by Pan and et al. [65] and Aziz-Kerzzo et al. [67] to simulate EIS data for an anodic oxide titanium film. This equivalent circuit is similar to shown in Fig. 1.1c, only in this R1 = Rs, which is electrolyte resistance, C1 = $C_{pr}$, which CPE of porous layer, R2 = $R_{pr}$, which is porous layer resistance, C2 = $C_b$, which CPE of barrier layer and R3 = $R_b$, which barrier layer resistance.

By evaluating $R_{pr}$ value at different anodizing potentials it gives data on the oxide film formed and namely if the $R_{pr}$ value is smaller than the pores produced should be larger. At the same time, Ti etching procedure before anodizing did not show any influence on Rpr values, but sealing of the oxide film increased $R_{pr}$ values [71]. This fact can be expected because $R_{pr}$ is associated to the outer porous layer resistance and sealing closes partially the film pores promoting a better behaviour of the anodised samples in terms of corrosion resistance. Etching of Ti surface and oxide film sealing instead increase $R_b$ values of samples. These facts could be an indication that the inner layer is also porous. Chemical etching causes a rougher Ti surface that might improve the barrier characteristic of the inner layer. Sealing in boiling deionized water converts amorphous Ti oxide into a more stable crystalline form. Thus, if the inner layer has pores the sealing process can improve the $R_b$ value, hence increases the inner layer corrosion resistance.

Over the years, fluoride containing electrolytes have been utilized to develop $TiO_2$ nanotubes of varied dimensions [72–74] in order to increase surface area for various applications. Based on EIS measurements in NaCl solution the presence of

inner barrier and outer porous $TiO_2$ nanotube layer was detected [75]. $TiO_2$ nanotubes showed two time constants at different frequency ranges and this can be due to the change in surface morphology and thickness changes with increasing anodization time. The decrease in phase angles at the high-frequency region may be related to the porous nature of the outer layer. Nyquist plots for as-formed and annealed $TiO_2$ nanotubes display a semicircle, which indicates near capacitive response and the presence of two time constants, can also be identified. Surface anodized for longer duration showed a larger capacitive loop which can be related to increase in thickness of the oxide layer. At high frequency, semicircles show that the transfer resistance dominates the impedance and at lower frequencies, Warburg impedance is observed which is due to diffusion of titanium ions to the porous layer. It has been reported that upon immersion in bio-fluids, Warburg impedance tends to decrease at earlier stages and finally it reaches a constant value. This behavior is due to the increase in the buildup of titanium ions in the electrolyte such that the diffusion of titanium ions back into the porous layer takes place.

More complex case is present by Suay et al. [55] which by means of electrochemical impedance spectra investigated composite process of aluminum porous anodizing, in the view of the sealing quality and the anodic films changes, and the ageing process produced by atmospheric exposure, which is important from the point of view of corrosion reliability of those oxides. To oversee the alumina porous film properties, it is a need to understand its nature. The hexagonal cells and barrier layer are made from anhydride alumina with different sulphate ions $Al_2(SO_4)_3$ from the anodizing bath. On the other hand, the porous layer is full of hydrate alumina (mono- or trihydrate or a mixture) plus absorbed water [55, 57]. Finally, there is one last layer (the intermediate layer), which is formed by diffusion from the exterior, especially in the sealing process, and slowly in atmospheric exposure [76]. Can be expected that significant changes in the porous layer will appear due to the atmospheric exposure (water absorption and the transformation of anhydride alumina to hydrate alumina inside the cells), and in the intermediate layer.

In order to fit the EIS experimental results of the anodic aluminum layer multipart equivalent circuit was proposed (Fig. 1.6). The parameter $R_{sol}$ represents

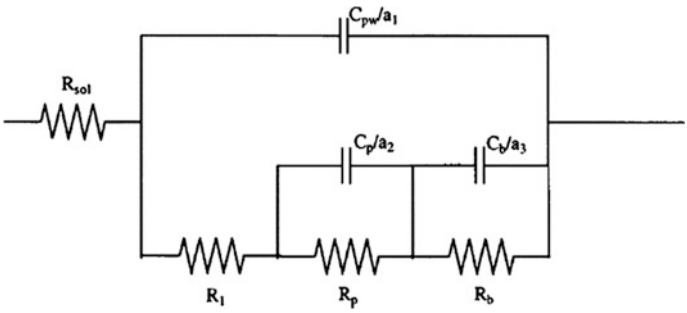


**Fig. 1.6** The proposed EC to model the impedance spectra of the sealed anodized aluminium layer

electrolyte used, $R_1$ simulates the presence of electrolyte in the pores and faults of the intermediate layer. One of the parallel branches which are present in the circuit is formed by the resistance $R_{pw}$ and the associate capacitance $C_{pw}$—they represent the walls of the hexagonal cells with uniform or nearly uniform dielectric properties. Taking into account that $R_{pw}$ is usually so high that it prevents the passage of current, so in equivalent circuit only a capacitance $C_{pw}$ in this branch is present. The other branch is formed by the resistance $R_1$ of the electrolyte in the pores and defects of the intermediate layer, in series with the pores as a whole (the pore and the barrier layers). The electrochemical properties of the pore filling are represented by $R_p$ and $C_p$, while the properties of the barrier layer are represented by $R_b$ and $C_b$.

Resistance $R_1$ is directly related to the intermediate layer changes as result to atmospheric exposure. $R_1$ vary markedly with the extent of sealing and the growing of the intermediate layer thickness (both processes are closely related and depend on ageing time) [55]. $R_1$ doubles in size for all types of atmospheres when the samples have been exposed up to 39 months. This change can be due to a better sealing of pores because hydroxides precipitation increases with exposure time and/or to an intermediate layer thickness increment. As exposure time increases precipitate particles start covering the alumina layer surface making cavities disappear and finally forming after years of exposure a homogeneous anodic layer surface, so anodized and sealed aluminum anticorrosion performance is increased due to sealing and natural ageing process.

A special case in the view of oxide films characterization by EIS is attributed to oxides formed on the metal/alloys surfaces. Here, we would like to point out oxides formed on nickel-based alloys, which are extensively used as component materials in nuclear power plants or in other aggressive corrosion environments due to its superior corrosion resistance that is attributed to the passive film formed on alloy surface. As surface metal oxide films exhibit a capacitive behavior, because of the dielectric nature of oxide films; therefore, it is convenient to study the structure of ones by EIS. During study of oxide films formed on the Ni-based superalloys in NaCl solutions was revealed a complex structure of ones that was reflected in EIS: there are three capacitance arcs in Bode plots [77]. The interfacial processes in the solutions were modeled by the equivalent circuit shown in Fig. 1.7. The values of the circuit element such as the solution resistance (Rs), the porous oxide capacitance (CPE1), the porous resistance (R1), the double layer capacitance (CPE2), the

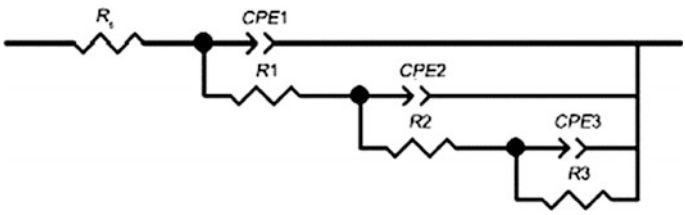


**Fig. 1.7** Equivalent circuit model employed in analysis of electrochemical impedance data of oxide films

compact resistance (R2), the compact oxide capacitance (CPE3) and polarization (the chloride ions transport) resistance (R3) were used to characterize the performance of the oxide film in the corrosive environment. Based on the changes in values of elements the following dynamics of processes was proposed. Diffusion of ions into micro-pores in the oxide film experienced difficulties because of the large resistance to charge transfer. Accordingly, the fitted resistance was very large. Under this condition, the changes of CPE3 with exposure time could be used to determine water/ions uptake of the oxide film. With increasing the immersion time, the oxide film capacitance (CPE3) increased, indicating that chloride ions had penetrated into the oxide film. After then, some interconnected micro-pores were filled with the electrolyte solution, which enables further measurements of the pores resistance reasonable.

The close dependence between breakdown of a passive film and its defective nature has been directly connected with its ionic and electronic conductivity characteristics [78]. Acquisition of Mott-Schottky plots is a usual way for semiconductor materials electrochemical characterisation such as semiconducting properties of the oxide film, such as the electronic type, the effective donor density and the flat band potential by measuring the electrode capacitance ($C$) as a function of the electrode potential ($E$). The capacitance as a function of the electrode potential ($E$) can be expressed as follows:

$$\frac{1}{C^2} = \frac{2}{\varepsilon\varepsilon_0 A^2 q N_q}\left(-E + E_{FB} + \frac{kT}{q}\right) \tag{1.25}$$

here ε and $\varepsilon_0$ is the dielectric constant of the passive film and permittivity vacuum, respectively, $q$ is the elementary charge ($-e$ for electron and $+e$ for holes), $N_q$ is the doping density which represents the donor $N_d$ or acceptor $N_a$ densities for and $n$- or $p$-type semiconductor; $q$ is the elementary charge ($-e$ for electron and $+e$ for holes), $k$ is the Boltzmann constant; $E_{FB}$ is the flat band potential; $A$ is area of electrode.

Therefore, a plot of $1/C^2$ against applied potential $E$ should yield a straight line from which $E_{FB}$ can be determined from the intercept on the $E$ axis, and the slope of line is equal to $\frac{2}{\varepsilon\varepsilon_0 A^2 q N_q}$ The value of $N_q$ can also be conveniently found from the slope knowing ε and A. Example of Mott-Schottky plot for passive film formed on stainless steel [79] in Fig. 1.8, and graph explaining how to extract parameters is presented in Fig. 1.9. Electrochemical determination of these parameters is simple when energy band edges are pinned at the surface and ac response of space charge layer capacitance can be separated in frequency range from other interfacial structures and processes, which is a usual case for stationary ideally polarisable semiconductor-electrolyte interface. Complications come with surface states and Faradaic processes that require frequency response analysis by impedance spectroscopy for extraction of space charge layer capacitance from the total ac response [80]. In this case the capacity can be extracted based on analysis of EIS data employed equivalent circuits containing capacity of double electric layer. The

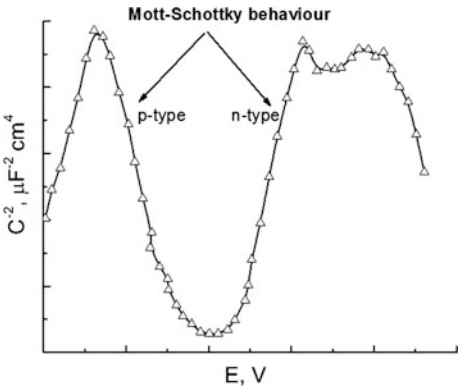


**Fig. 1.8** An example of Mott-Schottky plot for passive film

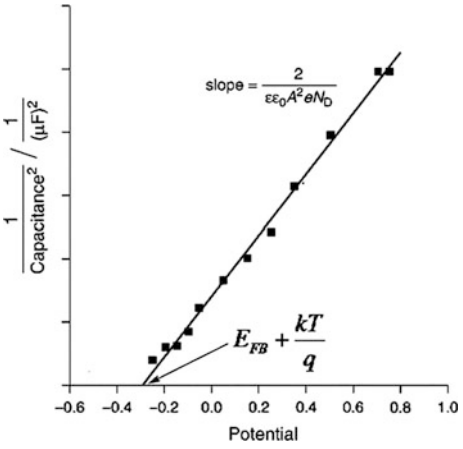


**Fig. 1.9** Determination parameters from Mott-Scottky plot

mentioned procedure using Randles equivalent circuit (see Fig. 1.1b) is described in [81].

As was shown in the case of Ni-based alloy [82], the slopes of straight lines in Mott-Schootky plots is tightly depended on the measured frequency, the slopes decrease with decreasing frequency, i.e., the capacitance decreases with increasing frequency. The source of the frequency dispersion is a matter of debate and various points of view is provided in this work. The main reason probably consists in frequency dispersion in Mott-Schottky tests aroused from surface roughness and inhomogeneous current flow. In some cases [75], the Mott-Schottky plot may show a wide variation in data with frequency for porous and defective oxide structures and makes it difficult to choose a frequency value for analysis. It has been recommended by authors [83, 84] that, a frequency greater than 1 kHz with relatively higher scan rate can be used to performMott Schottky analysis, where the ionic conductivity is negligible and the response is only due to electronic conductivity. The above equation shows a linear dependence between $C^{-2}$ and $E$. However,

non-linearity was observed experimentally, which according to Tomkiewicz [85] is due to oxidation of the electrode itself by holes in the depletion region, non-homogeneous doping and deep doping levels. Despite the existence of non-linear behavior, it has been shown that $N_D$ and $E_{FB}$ values can be determined fromthe slope and the intercept of the linear portion.

## 1.5 The Study of Underpotential Deposition of Metals by EIS

Underpotential deposition (UPD) is the phenomenon of electrochemical deposition of typically a monolayer of a metal on a foreign metal substrate at potentials higher than the reversible Nernst potential $E(Me^{n+}/Me)$, i.e. the deposition at "less negative" potential than that predicted from Nernst equation. In the wider sense, the UPD is not limited to the deposition of metals on metals; e.g. electrochemical adsorption of hydrogen atoms on platinum above $E(H^+/H_2)$ is also an example of UPD. The essence of the UPD phenomenon is in the surface limited character of the deposition. The UPD is controlled by the first atomic layer of the deposited material specific interaction with atoms of a substrate, which determines the intrinsic limit of the deposited material amount, typically a monolayer. Due to the surface limited character, the UPD is an efficient instrument for creating atomic layer building blocks for nanostructured materials assembly [86–91]. The UPD is also an important stage in the mechanisms of electrodeposition of semiconductor materials, mainly metal chalcogenides [92]. The difference between the reversible UPD potential, $E_{UPD}$ (or quasi-reversible potential in the case of irreversible UPD) and $E(Me^{n+}/Me)$ is called the UPD shift, $\Delta E_{UPD}$. The UPD shift correlates with differences of work functions of the substrate and the deposited metal in many UPD processes [93], though the correlation with work functions is not universal [94], e.g. in UPD of metals on tellurium $\Delta E_{UPD}$ shows correlation with free energies of formation of the corresponding tellurides rather than work function differences [95]. The dependences of the UPD shift on different physical quantities disclose possible differences in the nature of the interactions that control the underpotential deposition in different systems.

The surface limited character of the UPD determines the choice of electrochemical methods for investigation and monitoring of the underpotential deposition. The stationary electric current in the UPD is equal to zero, but the potentiodynamic profiles of the current and few other electrochemical variables obtained by potential sweep methods are typically very expressive (Fig. 1.10). The decay of the current at a steady potential under the potentiostatic control may affect essentially the frequency response acquired in impedance spectroscopy, due to the following reasons. First, the metal cation concentration profile which controls the impedance of diffusion decays along with the current. Second, many UPD processes are irreversible, i.e. the cathodic deposition and anodic oxidation of the

adlayer may proceed in different regions of potential, as shown in Fig. 1.10 for Pb UPD on tellurium. In the irreversible UPD, neither the forward, nor back reaction can respond to a small perturbation of the potential, when impedance spectrum is acquired at the steady state after the UPD current decay. So, the requirement of stationarity in the classical version of impedance spectroscopy appears to be in conflict with the essential properties of the object. The way out of this trouble is the same as in the case of voltammetric response acquisition in the UPD. Instead of measuring stationary frequency response which may lack essential contribution of the UPD, one can acquire the frequency response in the potential sweep, keeping in mind that the potential sweep itself causes a low-frequency limit in the frequency response acquisition [96]. Thus, the optimal solution in the UPD investigation by alternating current frequency response analysis lies in the use of potentiodynamic electrochemical impedance spectroscopy [96–98]. The latter is applicable both to reversible and irreversible UPD processes.

Interestingly, different equivalent electric circuits were derived from analysis of impedance spectra of reversible and irreversible UPD (Fig. 1.11) [96]. The equivalent circuit that represents typical reversible UPD processes (Fig. 1.12a) contains the charge transfer resistance $R_{ct}$, adsorption capacitance $C_a$ and Warburg impedance $Z_W$ in the Faradaic branch of the circuit, the latter is connected in parallel with double layer capacitance $C_{dl}$ and the two parallel branches are

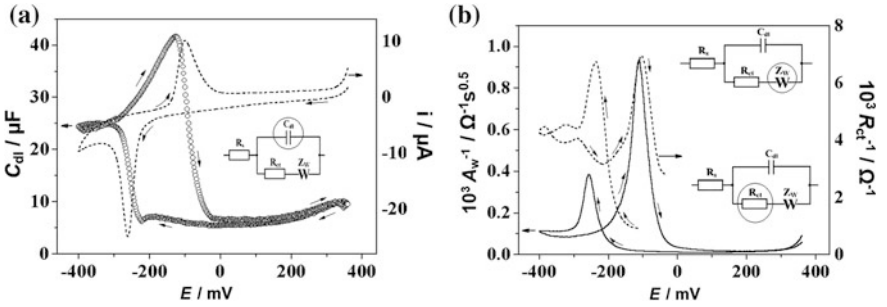


**Fig. 1.10** Potentiodynamic profiles of **a** electric current $i$ and double layer capacitance $C_{dl}$; **b** Warburg coefficient $A_W$ and charge transfer resistance $R_{ct}$ in Pb UPD on tellurium in 6 mM Pb $(NO_3)_2$ + 0.1 M $HNO_3$ at potential sweep rate 2.35 mV/s. The insets show equivalent electric circuits from which the frequency response parameters of the UPD were derived, with the corresponding elements of the circuit highlighted

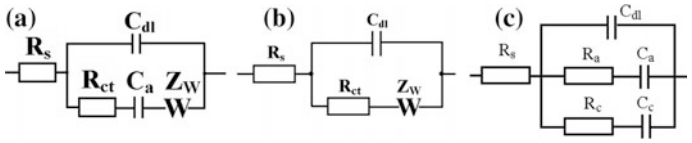


**Fig. 1.11** Basic equivalent electric circuits of **a** reversible, **b** irreversible UPD, and **c** the reversible UPD with anion coadsorption

altogether connected in series with the active resistance of solution $R_s$. The equivalent circuit of irreversible UPD contains the same elements except $C_a$ (Fig. 1.11b). The adsorption capacitance, which is characteristic only of the reversible UPD, results from oscillation of metal adatom coverage at the periodic perturbation of the potential. The adatom coverage does not oscillate in the absence of the back reaction; therefore, the irreversible UPD processes of the kind shown in Fig. 1.10 do not show this parameter.

The most informative parameter of the UPD derived from EIS is the double layer capacitance. This parameter discloses alterations of the interface status during the cathodic deposition and anodic oxidation of the adlayer (Fig. 1.10a). The two parameters of the Faradaic branch of the equivalent circuit, charge transfer resistance $R_p$ and Warburg coefficient σ, characterize, correspondingly, kinetic and diffusional contributions to the Faradaic impedance. The inverses of these two parameters show peaks at the potentials of adlayer deposition and oxidation (Fig. 1.10b).

In the case of a reversible UPD, the steady state coverage of the adatoms oscillates with the potential perturbation [99], so both versions of impedance spectroscopy can give informative frequency response which corresponds to either circuit *a*, or circuit *c* shown in Fig. 1.11. The circuit *c* characterises the UPD with coadsorption of anions, such as Bi [98, 99] or Cu [97] UPD on Au. The circuit *c* was first derived in the analysis of impedance spectra of hydrogen UPD on platinum [100]. The pseudocapacitances that result from UPD and also from anion coadsorption, when the latter affects the UPD, can be much higher than the double layer capacitance; however, their contribution to the total capacitive response of the electrode is graded by the charge transfer resistance that stands in series with the corresponding capacitance in the equivalent circuit. The adsorption capacitances can be also a valuable source of information about the UPD. Figure 1.12 shows the variation of the adsorption capacitance of lead UPD on gold in the cyclic scan and also the cyclic voltammograms of Pb UPD on bare gold and gold electrode covered with atomic layer of selenium [101]. The sharp peak in $C_a(E)$ plot in Fig. 1.12b discloses the phase transition in Pb monolayer in the final stage of UPD. This

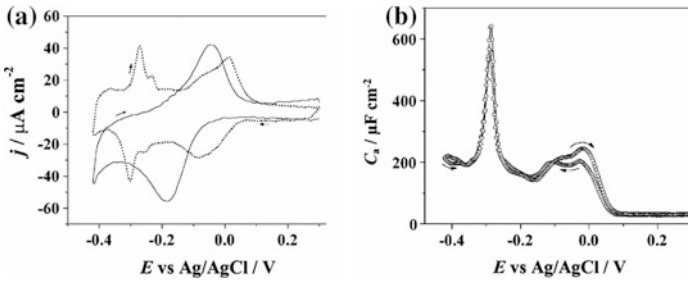


**Fig. 1.12** **a** Cyclic voltammograms of bare Au electrode (*dotted*) and Au electrode coated with selenium atomic layer (*solid*) in 1 mM $Pb(ClO_4)_2$ + 0.1 M $HClO_4$ and **b** the variation of lead adsorption pseudocapacitance in the cyclic scan that corresponds to the *dotted line* in *a*

element disappeared from the equivalent circuit of Pb UPD, after the gold electrode was covered electrochemically with atomic layer of selenium, which was due to the transition from reversible to irreversible UPD (see Fig. 1.12a).

Thus, impedance spectroscopy can be a very informative source of information about underpotential deposition when it is applied adequately with the account of the surface limited character of the UPD processes.

## 1.6 Characterization of Organic Films onto Metals by EIS

The base purpose of protective organic films is to prevent the corrosion of metal structures. New films are developed that could be more successfully resist the versatile aggressive environments to which metals are exposed during processing. In order to assist the development and characterization of new films formulations, the early evaluation of their performance is of greatest importance. This evaluation is possible by using electrochemical impedance spectroscopy (EIS).

The first works on the EIS characterization of organic films were published by Epelboin et al. [102] and Mansfield et al. [103], and it also suggested a general model of an equivalent electrical circuit from which a large number of other models can be derived. This circuit is composed of the electrolyte resistance, followed by a capacitance (coating capacitance *C*) in parallel with a resistance (the coating or pore resistance) and finally an element Z which represents the electrochemical impedance *Z* of the process at the metal interface. One of the simplest circuit describing *Z* is composed of a capacitance, which represents the double electric layer capacitance in parallel with a resistance representing charge transfer resistance, which describes the electrochemical reaction under activation control (Fig. 1.1c). This model "as is" (Fig. 1.1c) and with some modifications still is very popular and useful to investigate various systems containing organic films on the metallic surface, such as conducting polypyrrole film on Pt [104], fluor-polymer and oligomer coated steel [105–107], industrial lubricants on stainless steel [108], organic films and corrosion inhibitors [109–114].

One of the examples of such films can be used of organic films for steel protection. Interesting cases in this view presents the use of different "films-paints" [114–116]. Thus, research by EIS of the corrosion resistance of a water-based paint system applied on carbon steel is well documented [115, 116]. Epoxy-polyamine, epoxy-amine and epoxy-acrylic resins as primer films, and acrylic-polyurethane and acrylic paints as top films, were investigated both in single layer and double-layer applications. The best protection was provided by the epoxy-amine resin, whereas acrylic-polyurethane exhibited the poorest characteristics and signs of corrosion could be observed since the initial moments of immersion onwards. Even more efficient protection against corrosion can be provided by the acrylic polymer containing zinc phosphate pigments when it was applied as a multilayer system. In this way, the high density of pores produced in the polymer matrix during the curing process could be avoided to become direct ionic pathways for the transport of

aggressive species from the environment towards the surface of the underlying metal substrate [116].

Another case is use of oil lubricant films for steel protection. Fully formulated lubricant or organic films can be viewed as a non-aqueous colloidal polymeric system with low, primarily ionic electrical conductivity. Typical lubricating oil is composed of a combination of mineral or synthetic base oils and specialized additives designed to improve long-term stability and enhanced performance in aggressive environments. The dipolar nature of components of the lubricant permits investigation of their properties using electrochemical impedance spectroscopy. EIS presents an opportunity to resolve a complicated non-aqueous colloidal system both spatially and chemically, and to analyze specific parts of that system based on relaxation frequencies using small potential (5–10 mV) for the excitation of electrochemical activity of the system metal/coated film/solution. The final purpose of the EIS characterization of the protected organic coatings is to obtain information about the system properties such as presence of defects in films, reactivity of the interface, adhesion, barrier properties [113, 117].

Thus, one of the "oil films" which will be described here is barrier properties of the films of mineral oil SAE 10 with antioxidant as well as contained Fe particles were investigated [113]. The 3 cases of steel corrosion were investigated: (a) the steel corrosion without lubricant; (b) and (c)—oil film with and without suspended Fe particles, respectively. The oil film was formed on the active area of steel rod by dropping of fixed amount (5 μl) of oil. Such amount of oil allows forming of oil film with thickness 200–250 μm. As corrosive media for such kind of measurements usually NaCl solution is used.

The value of open circuit potential (OCP) is a parameter determined by the rates of cathodic reaction and anodic reaction of a corroding device. In the studying case, the cathodic reaction is hydrogen evolution reaction, and the anodic reaction is the active electrolytic dissolution of metal [118]. At the open circuit potential, the rates of these reactions are equal. The rates of both reactions depend on the corrosion media, chemical composition of electrode material. Furthermore, the hydrogen evolution reaction depends on the state of the surface. If oil film does not participate in any chemical interaction with steel, the OCP values should be close to each other both in the presence and absence of oil film. The data presented in Fig. 1.13 confirm this statement as settled values of OCP are in the range of $\sim$50–70 mV. The more positive values of OCP obtained for steel covered by film containing iron particles might be caused by contacting Fe particles whose surfaces are partially oxidized due to high specific area and activity. The OCP of oxidized entirely or in part surface is more positive than that for metallic surfaces. EIS is particularly well suited to evaluating corrosion behavior and insulator film characterization of materials whose surfaces have been coated with isolator films, because the EIS method in contrary to voltammetry is non-destructive method.

In Fig. 1.13 also Nyquist plots are presented for variously modified electrodes by oil films. To interpret data and physical meanings of the studied electrochemical system the equivalent circuit shown in Fig. 1.1c was used. This model is used in consideration that isolator film builds always on the metal surface in a corrosive

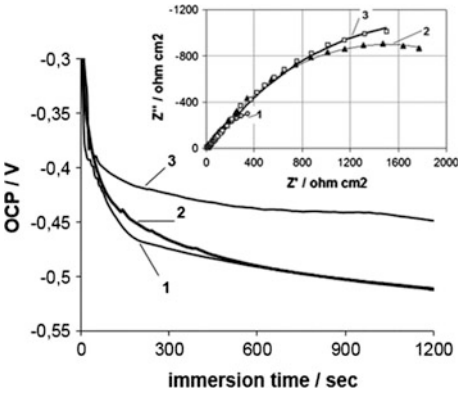


**Fig. 1.13** OCP versus time in 0.5 M NaCl solution and Nyquist plots of modified electrodes (*inset figure*). In both figures: *1*—bare steel electrode; *2*—steel covered with mineral oil film; *3*—steel covered with mineral oil + 0.1 % Fe film. *Inset figure* points—experimental data, solid lines—fitting results using equivalent circuit shown in Fig. 1.1c with values of elements presented in Table 1.1 and physical meaning as in [113])

environment. Thus, an equivalent circuit model for the metal-film-solution interface requires inclusion of the film parameters: R1 = $R_{sol}$, C1 = $CPE_{film}$, R2 = $R_{pores}$, C2 = CPE, R3 = $R_{corr}$, resistor, $R_{sol}$, is the bulk solution resistance [113]. This equivalent circuit is often used to interpret data obtained for metallic electrode coated by various organic films [110–113, 118–121]. The film resistor, $R_{pores}$, has been interpreted as the film resistance due to the electrolyte penetration through the porous film formed by fluor-oligomer. The film capacitor, $CPE_{film}$, has been interpreted as the capacitance of the electric capacitor consisting of film and the solution inside. $R_{corr}$ is the charge transfer resistance for the electrochemical reactions and in this case has a meaning of corrosion resistance. CPE in the real system is attributed to the non-ideal double layer capacitance separating the metal-electrolyte interface.

Resistances are more useful values to evaluate the corrosion behavior because charge transfer resistance ($R_{corr}$) which is inversely related to corrosion rate. As it follows from the data presented in Table 1.1, corrosion resistance is higher in the presence of oil (~2 times) and Fe particles in oil (~3 times). The film resistor $R_{pores}$ also is higher in the presence of oil films. The effectiveness of inhibition (*IE*) can be calculated from the values of charge transfer (corrosion) resistance by [113, 118]:

$$IE = \frac{R_{corr}^{film} - R_{corr}^{bare}}{R_{corr}^{film}} \cdot 100\,\%, \tag{1.26}$$

where: $R_{corr}^{film}$ is the charge transfer resistance in test with oil film; $R_{corr}^{bare}$ is the charge transfer resistance for bare electrode.

**Table 1.1** Values of elements used to fit experimental data with equivalent circuit shown in Fig. 1.1c

| Element | Bare steel | Steel covered with mineral oil film | Steel covered with mineral oil + 0.1 % Fe film |
|---|---|---|---|
| $R_{sol}$, Ω cm$^2$ | 3.84 | 4.97 | 4.28 |
| $R_{pores}$, Ω cm$^2$ | 63.99 | 278.6 | 490.4 |
| $R_{corr}$, Ω cm$^2$ | 1263 | 2683 | 3394 |
| $CPE_{film}$, μF cm$^{-2}$ | 19.40 | 21.35 | 34.92 |
| | n = 0.61 | n = 0.700 | n = 0.63 |
| $CPE$, μF cm$^{-2}$ | 53.20 | 15.20 | 21.24 |
| | n = 0.815 | n = 0.724 | n = 0.725 |

The IE in the 0.5 M NaCl of mineral oil film on steel is 53 %, and of mineral oil film containing Fe particles is 62 %. These results means that oil films are moderate corrosion inhibitors.

## 1.7 Electrochemical Impedance Spectroscopy (EIS) in Development of Biosensors and Biofuel Cells

EIS is has been successfully applied for the characterization of biosensing surfaces [122] and/or in evaluation of bioanalytical signals generated by biosensors [104].

Electrochemical biosensors could be divided into two principally different classes: (i) catalytic (which are mostly based on enzymatic catalysis) biosensors [123] and (ii) affinity sensors [124]. The application of EIS in both types of biosensors is significantly different, because in the most of enzymatic sensors variations that can be detected by EIS are mostly accumulated in bulk solution in the form of changing concentrations of reactants and/or reaction products, at the same time the changes on the enzyme-modified electrode are mostly not well detectable by EIS, therefore here other some electrochemical methods such as constant potential amperometry [125] or cyclic voltammetry are applied [126]. In this respect EIS is mostly applied during the formation of enzymatic and other materials based sub-layers, which are essential for function of the sensor, e.g. in our recent researches we have shown that EIS could be successfully applied for the evaluation of separateed multilayers in glucose sensors based on multi-layered structure [127, 128]. The EIS is mostly used in order to determine the double electric layer capacity and resistance of various modifiers, which carry the charge from electrolyte to electrode and also for the estimation of ion diffusion in solution towards the studied electrode [129]. Because of these abilities the EIS provides detailed information on some electrochemical characteristics of the electrochemical system. During our preliminary evaluation of 1,10-phenanthroline-5,6-dione and glucose oxidase modified electrode basic $R_\Omega(R_A C_A)$ circuit was applied [128],

however the circuit well fitted with experimental results only in very narrow frequency range from 1390 Hz to 14.37 mHz. Therefore, the aim of advanced research was advanced EIS-based evaluation of 1,10-phenanthroline-5,6-dione and glucose oxidase deposited on graphite electrodes, in order to adjust most suitable equivalent circuit, which is describing this electrochemical system [127]. It was determined that equivalent circuit $R_\Omega(R_{F2}C_2)(C[R_FW])$ most optimally describes this electrochemical system.

There are also some other studies on the application of EIS for the characterization of enzyme-modified surfaces [130]. Some other researches illustrated that EIS could be applied in glucose concentration measurements based on bio-electrochemical systems on GOx-modified electrodes [131].

Very different situation is observed in affinity sensors, because during the application of these sensors there are almost no observable changes in bulk solution, which could be easily detected by EIS. But differently from enzymatic biosensors in affinity sensors changes on electrode surface are very different since affinity sensors are not able to generate constant flow of electrons or significantly change the concentration of redox compound, therefore analytical signal in affinity sensors can be only indirectly detected by constant potential amperometry, e.g. such detection is possible when secondary antibodies labelled by horseradish peroxidase are applied [132]. However, surface changes in affinity sensors are significant therefore they could be determined and relatively well evaluated by various potentiodymic methods, such as cyclic voltammetry [133, 134], differential pulse voltammetry [134], square wave voltammetry [135], pulsed amperometric detection [136] and EIS techniques [134]. We have demonstrated that among here mentioned techniques EIS is providing the most useful set of data, which is required for the evaluation of analytical signal [134]. The EIS is based on electrochemical response of a system towards perturbations applied at different frequencies [104]. Using other electrochemical methods, such as amperometry or potentiometry there is always a problem of the measured system being non-linear because of changing electrochemical conditions, due to relatively high variation of electric current or voltage, and in this way influencing measured results. In potentiostatic EIS, which is based on constant electrode polarization voltage, a small sinusoidal perturbation of potential is usually applied. The amplitude of such perturbation usually is in the range of 5–20 mV. Such perturbation does not disturb the system's linearity and in this way it enables to acquire results, which are also linear in time and suitable for further analysis [129, 130]. Hence the EIS is one of the most informative out of many recently available electrochemical methods in development of affinity sensors and biosensors [135].

Especially well the EIS is applied in the sensors based on electrodes modified by semiconducting polymer based layers [137]. Especially well EIS is suitable for affinity sensors based on molecularly imprinted conducting polymers (MIPs) such as polypyrrole, which could be imprinted by low molecular mass molecules such as theophylline [138], caffeine [139, 140] or by large molecules such as proteins [141] and even DNA [142]. In a number of our research we have demonstrated that the EIS is the most efficient electrochemical signal detection technique in sensors where

here mentioned MIPs [138, 139, 142] or some other affinity towards analyte exhibiting structures are applied for creation of affinity sensors [143]. If correct equivalent circuit is applied the EIS has advantages over other electrochemical methods, (e.g. pulsed amperometric detection [136]).

It should be noted that conventional EIS based techniques represents only averaged response of the entire electrochemical system. Therefore, if advanced evaluation of affinity sensor signals is required during various stages of creation of affinity sensors [122, 139, 143, 144]. In such investigations combination of EIS with quartz crystal microbalances [139, 144], surface plasmon resonance [145], scanning electrochemical microscopy [122] and other techniques are applied.

In order to get more advanced mapping of electrochemical system the EIS could be merged with scanning electrochemical microscopy (SECM) this marged technique is named scanning electrochemical impedance spectroscopy (SEIM). In SEIM based technique localized impedance measurements could be performed in the range of frequencies when the surface of interest is scanned by ultramicroelectrode (UME) [122]. Dependingly on requerments the result of SEIM could be visualized by mapping one of calculated parameters, e.g. charge transfer resistance or double layer capacitance as a function of 3D coordinates [146, 147]. It was demonstrated that the combination of SECM and EIS is providing information about local corrosion phenomena, which could help to identify the location of defects induced by corrosion [147]. In addition, comparison of conventional EIS with localized EIS was done during the investigation of degradation of polyester coil-coated galvanized steel [148] and in the evaluation of the degradation of some coatings, which were based on deposited organic compounds or polymeric layers [149, 150].

During the development of enzymatic biosensors, it was demonstrated that the glucose oxidase (GOx) based biosensor surfaces could be sucessfully analyzed by merged scanning electrochemical microscopy (SECM) and EIS techniques [122]. This advancement of SECM by EIS could provide additional electrochemical information on electrochemical properties and concentrations gradients of electrochemically active and even not active materials in selected 3D volume of solution [122]. Such EIS data based information could be very atractive in the evaluation of biofuel cell efficiency [151] and in the modelling of biosensor action [152] because it is hardly available by other electrochemical methods.

The evaluation of enzymatic reaction intensity could be estimated by conventional SECM techniques [153, 154]. However, in conventional SECM the most commonly used electrochemical method is based on faradaic response when fixed potential is applied to the UME in order to register the concentration of electrochemically active enzymatic reaction products [155, 156]. Moreover, it should be noted, that the potential applied to the electrode drives the electrochemical system far from the equilibrium, and then the response to this perturbation is observed as disturbing signal. In order to avoid this problem, the applicability of technique based on SECM in which the UME is modulated by selected frequency alternating current (AC-SECM) can be applied. The AC-SECM based technique also allows to study local corrosion processes in the entire solution volume without any redox

mediator [157]. Using AC-SECM method the approach curves were recorded at several different frequencies and they demonstrated negative feedback behavior while the UME was approaching an insulating surface [158]. This phenomenon is similar to that observed in faradaic SECM based methods, however, different approach curves were observed when different frequencies were applied [159]. In order to advance this technique, the entire electrochemical impedance spectra can be registered at every measurement point and then the electrochemical system can be evaluated using the most suitable and informative equivalent circuits. This technique is called scanning electrochemical impedance microscopy (SEIM). In the case of SEIM conventional approach curves, which represent ohmic resistance and/or other equivalent circuit parameters vs distance are plotted. The concept of SEIM was described recently in the evaluation of localized corrosion processes by Schuhmann's group [147, 160]. When SEIM was applied for localized evaluation of corrosion processes the sample was minimally influenced by UME, which was applied as a scanning probe, and it was demonstrated that domains, which have different electrochemical properties, could be easily distinguished by SEIM even if they have similar topography and/or morphology [147]. In another research, impedance dependence on UME distance from insulating sample was revealed at feedback mode SEIM [161]. The spherical diffusion, which has most significant influence far from insulating surface, was evaluated by Cole-Cole impedance evaluation method, and the radial diffusion, which has most significant influence when the UME is approaching insulating surface, was evaluated by Cole-Davidson impedance evaluation method. It was determined that the low-frequency part of the EIS in a thin-layer between UME and surface of interest is controlled by both above mentioned types of diffusion. Moreover, it was also demonstrated that the SEIM in feedback mode is suitable for constant-height based imaging. When SEIM was acting in feedback mode the local information on both topography and surface reactivity was obtained from the simultaneous analysis of the current and electrolyte-resistance variations [162]. Fundamental aspects of SEIM were investigated comparing UME responses while it was approaching to different surfaces e.g.: (i) insulator surface, (ii) conducting surface not-connected to electric circuit, and (iii) conducting surface, which was connected to electric circuit and was held at constant potential [163]. By this research it has been shown that the admittance of the UME located at relatively small distance from the surface of interest mostly depends on the distance between UME and the surface and on interfacial properties of the surface. Therefore, the SEIM based imaging is informative even without any redox mediators. When AC-SECM and SECM methods are compared, it should be noted that the AC-SECM is performed at single frequency, while the SEIM is performed in broad range of frequencies what enables to select the most suitable equivalent circuit and to calculate number of EIS parameters. Therefore, parameters, which are derived from SEIM evaluations, better describe an electrochemical system than the parameters that are derived from AC-SECM data. We believe that the SEIM could be suitable for the investigation of biosensor and biofuel cell surfaces in order to evaluate localized activity of immobilized enzymes and/or to perform advanced evaluation of the diffusion of enzymatic reaction products.

Some researches were based on the EIS application for the evaluation of enzymatic reaction when the enzymes were immobilized on surfaces of electrodes [127, 128]. In addition, it was determined that conventional SECM is very suitable for the investigation of enzyme-modified insulating surfaces while applying constant potential to UME [153–156]. Therefore, by the assumption of previous achievements we have expected that it is possible to merge the EIS technique with SECM in order to get efficient SEIM system, which will be suitable for the evaluation of enzyme-modified surfaces [122]. The main aim of here mentioned research was to merge EIS with SECM into efficient SEIM system and, using developed SEIM for the investigation of solution conductivity at different positions, to demonstrate the suitability of SEIM for the evaluation of reaction product diffusion from enzyme-modified surface in real time [22]. The working electrode in this research applied SEIM equipment was an UME. This electrode was scanning in all three directions and therefore it was applied for the investigation of selected 3D space of solution. The obtained data were analyzed using randles equivalent circuit. Actually the SEIM is used more rarely, than the AC-SECM, because scanning at one desired frequency takes less time. But the advantage of SEIM is that the EIS measurements are performed in wide range of frequencies at each point of the UME position. Such measurements allow to evaluate the response of the electrochemical system, to develop 3D model of the system, also to determine the most suitable equivalent circuit and their parameters, which in the most optimal way to describe the system [125]. What is the most important, such measurements allow to find the values of equivalent circuit parameters in selected volume of the electrochemical cell. Reaction products, which affect solution's conductivity, diffuse from the active sites of GOx-modified surface into the solution; therefore, the SEIM with moving UME is one of the best choice to study the diffusion of formed reaction products in selected volume of electrochemical cell. Due to the fact that the EIS measurements take a long time, the conductivity changes in time were also evaluated and this issue was taken into account.

Another alternative technique, which is used for the determination of localized EIS data, is an impedance imaging combined with atomic force scanning electrochemical microscopy (AFM-SECM) [164]. In this technique the AFM-based topography and alternating current SECM (AC–SECM) based signals are recorded simultaneously with ring-shaped microelectrode, which is integrated on the AFM probe. In one AC–SECM-based research structured glass/gold substrate was evaluated by such advanced AFM probe and significant increase of current was registered when the probe was placed over spots consisting of gold [164].

However, according to our best knowledge, up to now complex research in the area of application of EIS for the investigation of biosensors and biofuel cells is still missing. Therefore, despite of high number of researches based on various EIS applications in biosensorics and biofuel cell development, further developments in these areas are required especially in those directions where the combination with other surface characterization techniques is leading towards advanced phenomena of complex interactions between biomolecules and modified electrode.

## 1.8 Conclusions

1. Electrochemical impedance spectroscopy (EIS) is a recent and powerful tool in corrosion and solid state laboratories. The basics of EIS and data presentation formats (Nyquist, Cole-Cole, Bode) are described and discussed.
2. The described interpretation of EIS data is built upon equivalent circuit. Regardless the variety of electrode processes its contain the similar stages and comprises similar processes such as formation of double electric layer, the presence of ohmic resistance, charge transfer resistance of electrochemical reaction, and etc. Therefore, the same equivalent circuits but with some special physical meaning of passive elements of equivalent circuit can simulate the various processes occurred on the electrode, such as cathodic metals/alloys films deposition; anodization of metals, under potential deposition of metals; characterization of organic films onto metals, application in development of biosensors and biofuel cells. With the equations of the model it is then possible to calculate the electrochemical impedance as a function of frequency and check conformity experimental data to theoretical model using commercial software.
3. Combining study by scanning electrochemical microscopy and EIS could be very attractive in order to evaluate the biofuel cell efficiency and in the modeling of biosensor action as it is unavailable to obtain by other convenient electrochemical methods.

**Acknowledgments** The authors acknowledge funding from FP7 Oil&Sugar project (295202), from the Research Council of Lithuania (MIP-031/2014) and Moldavian national projects (15.817.02.05A), (14.819.02.16F). Also, A.Ramanavicius is grateful to LaMeTech program project No.VP1-3.1-SMM-08-K-01-004/KS-120000-1756 for financial support.

## References

1. M. Sluyters-Rehbah, Impedances of electrochemical systems: terminology, nomenclature and representation. Part 1. Cells with metal electrodes and liquid solutions. Pure Appl. Chem. **66** (9), 1831–1891 (1994)
2. A.J. Bard, L.R. Faulkner, Electrochemical methods. *Fundamentals and Applications* (Wiley, New York, 2001), 829 pp
3. E. Barsoukov, J.R. Macdonald (ed.), *Impedance Spectroscopy Theory, Experiment, and Applications* (Wiley, New York, 2005), 595 pp
4. M.E. Orazem, B. Tribollet, *Electrochemical Impedance Spectroscopy* (Wiley, New York, 2008), 523 pp
5. A. Lasia, in *Electrochemical Impedance Spectroscopy and its Applications*, ed. by B.E. Conway, J.O'M. Bockris, R.E. White, Modern Aspects of Electrochemistry, vol. 32 (Kluwer Academic Publishers, New York), pp. 143–248
6. A. Lasia, *Electrochemical Impedance Spectroscopy and its Applications* (Springer, New York, 2014), 367 pp
7. D. Landoldt, *Corrosion and Surface Chemistry of Metals* (EPFL Press, Lausanne, 2007), 622 pp

8. J.O'M Bockris, A.K.N. Reddy, M. Gamboa-Aldeco, *Modern Electrochemistry*, vol. 24. Fundamentals of Electrodics (Kluwer Academic Publishers, New York, 2002)
9. N. Tsyntsaru, H. Cesiulis, M. Donten, J. Sorte, E. Pellicer, E.J. Podlaha-Murphy, Modern trends in tungsten alloys electrodeposition with iron group metals. Surf. Eng. Appl. Electrochem. **48**(6), 491–520 (2012)
10. S.S. Belevskii, H. Cesiulis, N. Tsyntsaru, A.I. Dikusar, The role of mass transfer in the formation of the composition and structure of CoW coatings electrodeposited from citrate solutions. Surf. Eng. Appl. Electrochem. **46**(6), 570–578 (2010)
11. Y. Liu, W. Wangz, Investigation on the Cu(II) and Co(II) electrochemical reduction process in citrate solution by CV and EIS. J. Electrochem. Soc. **159**(6), D375–D381 (2012)
12. T. Pajkossy, Th Wandlowski, D.M. Kolb, Impedance aspects of the anion adsorption on gold single crystal electrodes. J. Electroanal. Chem. **414**, 209–220 (1996)
13. J.R. Macdonald, *Impedance Spectroscopy Emphasizing Solid Materials and Systems* (Wiley, New York, 1987)
14. C. Cachet, B. Saidani, R. Wiart, A model for zinc deposition in alkaline electrolytes: inhibition layer and activation mechanism. Electrochim. Acta **34**, 1249 (1989)
15. C. Cachet, B. Saidani, R. Wiart, The kinetics of zinc deposition at low overpotentials in alkaline electrolytes. Electrochim. Acta **33**, 405 (1988)
16. C. Cachet, B. Saidani, R. Wiart, The behavior of zinc electrode in alkaline electrolytes I. A kinetic analysis of cathodic deposition. J. Electrochem. Soc. **138**, 678 (1991)
17. C. Cachet, Z. Chami, R. Wiart, The behavior of zinc electrode in alkaline electrolytes II. A kinetic analysis of anodic dissolution. J. Electrochem. Soc. **139**(3), 644–654 (1991)
18. T. Chengyu, C. Hang, H. Wei, L. Yu, Z. Ziqiao, Influence of Nano-$Al_2O_3$ particles on nickel electrocrystallization at initial stage. Rare Metal Mat. Eng. **39**, 10–16 (2010)
19. C. Cachet, C. Gabrielli, F. Huet, M. Keddam, R. Wiart, Electrochim. Acta **28**, 899 (1983)
20. I. Danaee, Theoretical and experimental studies of layer by layer nucleation and growth of palladium on stainless steel Chemija. **24**(2), 128–136 (2013)
21. E.M. Garcia, T. Matencio, R.Z. Domingues, L.M. Garcia, J.A. Figueiredo dos Santos, N. Ribeiro, H.A. Tarôco, V. F.C. Lins, Study of cobalt electrodeposition onto stainless steel using electrochemical impedance spectroscopy (IES) J. Phys. Sci. Appl. **2**(10), 409–413 (2012)
22. E. Lassner, W.D. Schubert, *Tungsten—Properties, Chemistry, Technology of the Element, Alloys, and Chemical Compounds* (Springer, New York, 1999), 422 pp
23. M. Schwartz, N.V. Myung, K. Nobe, Electrodeposition of iron group-rare earth alloys from aqueous media. J. Electrochem. Soc. **151**, C468–C477 (2004)
24. H. Cesiulis, A. Baltutiene, M. Donten, M.L. Donten, Z. Stojek, Increase in rate of electrodeposition and in Ni(II) concentration in the bath as a way to control grain size of amorphous/nanocrystalline Ni-W alloys. J. Solid State Electrochem. **6**, 237–244 (2002)
25. H. Cesiulis, E.J. Podlaha-Murphy, Electrolyte considerations of electrodeposited Ni-W alloys for microdevice fabrication. Mater. Sci. (Medziagotyra) **9**, 324–327 (2003)
26. H. Cesiulis, M. Donten, M.L. Donten, Z. Stojek, Electrodeposition of Ni-W Ni-Mo and Ni-Mo-W alloys from pyrophosphate baths. Mater. Sci. (Medziagotyra) **7**, 237–241 (2001)
27. P. Andricacos, S.H. Boettcher, S.G. Malhotra, M. Paunovic, C. Ransom, Structure comprising a barrier layer of a tungsten alloy comprising cobalt and/or nickel. U.S. Patent Application Publication 6 pp. US 2004108136 A1 20040610 (2004)
28. M. Svensson, U. Wahlstrom, G. Holmbom, Compositionally modulated cobalt–tungsten alloys deposited from a single ammoniacal electrolyte. Surf. Coat. Technol. **105**, 218–223 (1998)
29. G.Y. Wei, J.W. Lou, H.L. Ge, Y.D. Yu, L. Jiang, L.X. Sun, Co–W films prepared from electroplating baths with different complexing agents. Surf. Eng. **28**, 412–417 (2012)
30. D.P. Weston, S.J. Harris, P.H. Shipway, N.J. Weston, G.N. Yap, Establishing relationships between bath chemistry, electrodeposition and microstructure of Co-W alloy coatings produced from a gluconate bath. Electrochim. Acta **55**, 5695–5708 (2010)

31. D.P. Weston, S.J. Haris, H. Capel, N. Ahmed, P.H. Shipway, J.M. Yellup, Nanostructured Co-W coatings produced by electrodeposition to replace hard Cr on aerospace components. Trans. Inst. Metal Finish. **88**, 47–56 (2010)
32. A.I. Shul'man, S.S. Belevskii, S.P. Yushchenko, A.I. Dikusar, Role of complexation in forming composition of Co-W coatings electrodeposited from gluconate electrolyte. Surf. Eng. Appl. Electrochem. **50**(1), 9–17 (2014)
33. S.S. Belevskii, S.P. Yushchenko, A.I. Dikusar, Anomalous electrodeposition of Co-W coatings from a citrate electrolyte due to the formation of multinuclear heterometallic complexes in the solution. Surf. Eng. Appl. Electrochem. **48**, 97–98 (2012)
34. J.S. Santos, F. Trivinho-Strixino, E.C. Pereira, Investigation of Co(OH)2 formation during cobalt electrodeposition using a chemometric procedure. Surf. Coat. Technol. **205**, 2585–2589 (2010)
35. P. Vermeiren, R. Leysen, H. Vandenborre, Study of hydrogen evolving reaction in alkaline medium at nickel and cobalt based electrocatalysts. Electrochim. Acta **30**, 1253 (1985)
36. D.R. Gabe, The role of hydrogen in metal electrodeposition processes. J. Appl. Electrochem. **27**, 908 (1997)
37. J.T. Matsushima, F. Trivinho-Strixino, E.C. Pereira, Investigation of cobalt deposition using the electrochemical quartz crystal microbalance Electrochim. Acta **51** (2006)
38. J.S. Santos, R. Matos, F. Trivinho-Strixino, E.C. Pereira, Effect of temperature on Co electrodeposition in the presence of boric acid Electrochim. Acta **53**, 644 (2007)
39. W.C. Grande, J.B. Talbot, Electrodeposition of thin films of nickel-iron. 1. Experimental. J. Electrochem. Soc. **140**(3), 669–674 (1993)
40. W.C. Grande, J.B. Talbot, Electrodeposition of thin films of nickel-iron. 2. Modelling. J. Electrochem. Soc. **140**(3), 675–681 (1993)
41. A. Budreika, The study of the electrodeposition of Ni, Co and their alloys with tungsten and molybdenum. Doctoral dissertation, 2010, Vilnius
42. Yan Liu, Wei Wang, Investigation on the Cu(II) and Co(II) electrochemical reduction process in citrate solution by CV and EIS. J. Electrochem. Soc. **159**(6), D375–D381 (2012)
43. H. Cesiulis, G. Baltrunas, The study of surface passivity and blocking by the electrochemical technique. Physicochem. Mech. Mater. **5**, 11–17 (2006)
44. M.I. Jeffrey, W.L. Choo, P.L. Breuer, The effect of additives and impurities on the cobalt electrowinning process. Miner. Eng. **13**(12), 1231–1241 (2000)
45. S.S. Belevskii, S.P. Yushchenko, A.I. Dikusar, Electrodeposition of nanocrystalline Co–W coatings from citrate electrolytes under controlled hydrodynamic conditions: Part 1. Co electrodeposition. Surf. Eng. Appl. Electrochem. **45**(6), 446–454 (2009)
46. S.S. Belevskii, N.I. Tsyntsaru, A.I. Dikusar, Electrodeposition of nanocrystalline Co–W coatings from citrate electrolytes under controlled hydrodynamic conditions: part 2. The electrodeposition rate and composition of the coatings. Surf. Eng. Appl. Electrochem. **46**(2), 91–99 (2010)
47. N. Tsyntsaru, H. Cesiulis, E. Pellicer, J.-P. Celis, J. Sort, Structural, magnetic, and mechanical properties of electrodepositedcobalt–tungsten alloys: intrinsic and extrinsic interdependencies. Electrochim. Acta **104**, 94–103 (2013)
48. S.A. Silkin, S.S. Belevskii, A.S. Gradinar, V.I. Petrenko, I.V. Yakovets, N.I. Tsyntsaru, A.I. Dikusar, Electrodeposition of nanocrystalline Co–W coatings from citrate electrolytes under controlled hydrodynamic conditions: part 3. The micro_ and macrodistribution of the deposition rates, the structure and the mechanical properties. Surf. Eng. Appl. Electrochem. **46**(3), 206–214 (2010)
49. L.M. Hagelsieb, Anodic aluminum oxide processing, characterization and application to DNA hybridization electrical detection. PhD. thesis, Universite Catholique de Louvain, Louvain-La-Neuve, Belgique (2007)
50. C.X. Jiang, J.P. Tu, S.Y. Guo, M.F. Fu, X.B. Zhao, Friction properties of oil-infiltrated porous AAO film on an aluminium substrate. Acta Metallurgica Sinica (English Letters) **18**, 249–253 (2005)

51. W. Lee, The anodization of aluminium for nanotechnology applications. JOM **62**, 57–63 (2010)
52. J. Choi, Fabrication of monodomain porous alumina using nanoimprint lithography and its applications. PhD. thesis, Martin-Luther-Universitat Halle, Wittenberg, Germany (2004)
53. I.U. Khan, P. John, S.T. Sheikh, N. Gulzar, A.U. Rehman, Anodizing of aluminum with improved corrosion properties. J. Chem. Soc. Pak. **32**, 46–51 (2010)
54. T.D. Burleigh, P. Schmuki, S. Virtanen, Properties of the nanoporous anodic oxide electrochemically grown on steel in hot 50 % NaOH. J. Electrochem. Soc. **156**(1), C45–C53 (2009)
55. J.J. Suay, E. Gimenez, T. Rodrıguez, K. Habbib, J.J. Saura, Characterization of anodized and sealed aluminium by EIS. Corros. Sci. **45**, 611–624 (2003)
56. M.R. Kalantary, D.R. Gabe, D.H. Ross, A model for the mechanism of nickel fluoride cold sealing of anodized aluminium. J. Appl. Electrochem. **22**(3), 268–276 (1992)
57. J.A. Gonzalez, S. Feliu, J.A. Bautista, E. Otero, Changes in cold sealed aluminum oxide films during ageing. J. Appl. Electrochem. **29**, 843–852 (1999)
58. V López, E. Otero, A. Bautista, E. Escudero, J.A. González, Changes in the morphology of porous anodic films formed on aluminium in natural and artificial ageing. Rev Metal Madrid Vol Extr, 104–109 (2003)
59. F. Mansfeld, M.W. Kendig, Spectroscopy as quality control and corrosion test for anodized aluminum alloys. Corrosion **41**, 490 (1985)
60. F. Mansfeld, M.W. Kendig, W.J. Lorenz, Corrosion inhibition in neutral, aerated media. J. Electrochem. Soc. **132**, 290 (1985)
61. J. Hizing, K. Juettner, W.J. Lorenz, W. Paatsch, AC-impedance measurements on porous aluminium oxide films. Corros. Sci. **24**, 945 (1984)
62. T.P. Hoar, G.C. Wood, The sealing of porous anodic oxide films on aluminium. Electrochim. Acta **7**, 333 (1962)
63. K. Juettner, W.J. Lorenz, W. Paatsch, The role of surface inhomogeneities in corrosion processes-electrochemical impedance spectroscopy (EIS) on different aluminium oxide films. Corros. Sci. **29**, 279–288 (1989)
64. F. Mansfeld, Electrochemical impedance spectroscopy (EIS) as a new tool for investigating methods of corrosion protection. Electrochim. Acta **35**, 1533 (1990)
65. J. Pan, D. Thierry, C. Leygraf, Electrochemical impedance spectroscopy study of the passive oxide film on titanium for implant application. Electrochim. Acta **41**(7–8), 1143 (1996)
66. J.R. Birch, T.D. Burleigh, Oxides formed on titanum by polishing, etching, anodzng, or thermal oxidizng. Corrosion **56**(12), 1233 (2000)
67. M. Aziz-Kerrzo, K.G. Conroy, A.M. Fenelon, S.T. Farrell, C.B. Breslin, Electrochemical studies on the stability and corrosion resistance of titanium-based implant materials. Biomaterials **22**, 1531 (2001)
68. S. Piazza, G. Lo, Biundo, M.C. Romano, C. Sunseri, F. Di Quarto, In situ characterization of passive films on al-ti alloy by photocurrent and impedance spectroscopyfn1. Corros. Sci. **40** (7), 1087 (1998)
69. J.R. Macdonald, *Impedance Spectroscopy* (Wiley, New York, 1987)
70. M.J. Esplandiu, E.M. Patrito, V.A. Macagno, Characterization of hafnium anodic oxide films: an AC impedance investigation. Electrochim. Acta **40**(7), 809 (1995)
71. M.E.P. Souza, M. Ballester, C.M.A. Freire, EIS characterisation of Ti anodic oxide porous films formed using modulated potential. Surf. Coat. Technol. **201**, 7775–7780 (2007)
72. J.M. Macak, L.V. Taveira, H. Tsuchiya, K. Sirotna, J. Macak, P. Schmuki, Influence of different fluoride containing electrolytes on the formation of self-organized titania nanotubes by Ti anodization. J. Electroceram. **16**, 29–34 (2006)
73. N.K. Shrestha, J.M. Macak, F. Schmidt-Stein, R. Hahn, C.T. Mierke, B. Fabry, P. Schmuki, Magnetically guided titania nanotubes for site-selective photocatalysis and drug release. Angew. Chem. **120**, 1–5 (2008)

74. H. Cesiulis, T. Maliar, N. Tsyntsaru, F. Wenger, P. Ponthiaux, E. Podlaha, Anodic titanium oxide films: photoelectrochemical and tribocorrosion behavior. J. Nanoelectron. Optoelectron. **9**, 1–6 (2014)
75. Balakrishnan Munirathinam, Lakshman Neelakantan, Titania nanotubes from weak organic acid electrolyte: Fabrication, characterization and oxide film properties. Mater. Sci. Eng. C **49**, 567–578 (2015)
76. A.W. Brace, *The Technology of Anodizing Aluminium* (Tecnicopy Ltd., Stonenhouse, Gloucesterhire, Great Britian, 1979), pp. 1–19
77. H. Bai, F. Wang, Protective properties of high temperature oxide films on Ni-based superalloys in 3.5 % NaCl solution. J. Mater. Sci. Technol. **23**(4) (2007)
78. P. Schmuki, H. Bohni, Semiconductive properties of passive films and susceptibility to localized corrosion. Werkstoffe und Korrosion Mater. Corros. **42**(5), 203–207 (1991)
79. N.E. Hakiki, S. Boudin, B. Rondot, M. Da Cunha, Belo. The electronic structure of passive films formed on stainless steels. Corros. Sci. **37**(11), 1809–1822 (1995)
80. A.S. Bondarenko, G.A. Ragoisha. Variable Mott-Schottky plots acquisition by potentiodynamic electrochemical impedance spectroscopy. J. Solid State Electrochem. **9** (12), 845–849 (2005)
81. K. Gelderman, L. Lee, S.W. Donne, Flat-band potential of a semiconductor: using the Mott-Schottky equation. J. Chem. Educ. **84**(7), 685–688 (2007)
82. D. Li, D. Chen, J. Wang, H. Chen, Chemical composition and Mott-Schottky analysis of passive film formed on G3 alloy in bicarbonate/karbonate buffer solution. Acta Metall. Sin. (Engl. Lett.). **23**(6), 461–472 (2010)
83. E. Sikora, J. Sikora, D.D. Macdonald, A new method for estimating the diffusivities of vacancies in passive films. Electrochim. Acta **41**(6), 783–789 (1996)
84. Z. Jiang, X. Dai, H. Middleton, Investigation on passivity of titanium under steady-state conditions in acidic solutions. Mater. Chem. Phys. **126**(3), 859–865 (2011)
85. M. Tomkiewicz, Impedance spectroscopy of rectifying semiconductor-electrolyte interfaces. Electrochim. Acta **35**(10), 1631–1635 (1990)
86. B.W. Gregory, D.W. Suggs, J.L. Stickney, Conditions for the deposition of CdTe by electrochemical atomic layer epitaxy. J. Electrochem. Soc. **138**, 1279–1284 (1991)
87. F. Forni, M. Innocenti, G. Pezzatini, M.L. Foresti, Electrochemical aspects of CdTe growth on the face (111) of silver by ECALE. Electrochim. Acta **45**, 3225–3231 (2000)
88. A.S. Bondarenko, G.A. Ragoisha, N.P. Osipovich, E.A. Streltsov, Multiparametric electrochemical characterisation of Te-Cu-Pb atomic three-layer structure deposition on polycrystalline gold. Electrochem. Commun. **8**, 921–926 (2006)
89. G.A. Ragoisha, A.S. Bondarenko, N.P. Osipovich, S.M. Rabchynski, E.A. Streltsov, Multiparametric characterisation of metal-chalcogen atomic multilayer assembly by potentiodynamic electrochemical impedance spectroscopy. Electrochim. Acta **53**, 3879–3888 (2008)
90. I. Sisman, U. Demir, Electrochemical growth and characterization of size-quantized CdTe thin films grown by underpotential deposition. J. Electroanal. Chem. **651**, 222–227 (2011)
91. J. Stickney, in *Encyclopedia of Applied Electrochemistry*, ed. by G. Kreysa, R.F. Savinell, K. Ota (Springer, New York, 2014), pp. 1447–1453
92. M. Bouroushian, *Electrochemistry of Metal Chalcogenides* (Springer, Heidelberg, 2010)
93. D.M. Kolb, M. Przasnysky, H. Gerischer, Underpotential deposition of metals and work function differences. J. Electroanal. Chem. **54**, 25–38 (1974)
94. E. Budevski, G. Staikov, W.J. Lorenz, *Electrochemical Phase Formation and Growth* (VCH, Weinheim, 1996)
95. P.V. Chulkin, Y.M. Aniskevich, E.A. Streltsov, G.A. Ragoisha, Underpotential shift in electrodeposition of metal adlayer on tellurium and the free energy of metal telluride formation. J Solid State Electrochem. **19**, 2511–2516 (2015). doi:10.1007/s10008-015-2831-x
96. G.A. Ragoisha, Potentiodynamic electrochemical impedance spectroscopy for underpotential deposition processes. Electroanalysis **27**, 855–863 (2015)

97. G.A. Ragoisha, A.S. Bondarenko, Potentiodynamic electrochemical impedance spectroscopy. Copper underpotential deposition on gold. Electrochem. Commun. **5**, 392–395 (2003)
98. G.A. Ragoisha, A.S. Bondarenko, Potentiodynamic electrochemical impedance spectroscopy. Electrochim. Acta **50**, 1553–1563 (2005)
99. J.E. Garland, K.A. Assiongbon, C.M. Pettit, S.B. Emery, D. Roy, Kinetic analysis of electrosorption using fast fourier transform electrochemical impedance spectroscopy: underpotential deposition of $Bi^{3+}$ in the presence of coadsorbing $ClO^{4-}$ on Gold. Electrochim. Acta **47**, 4113–4124 (2002)
100. S. Morin, H. Dumont, B.E. Conway, Evaluation of the effect of 2-Dimensional geometry of Pt single-crystal faces on the kinetics of UPD of H using impedance spectroscopy. J. Electroanal. Chem. **412**, 39–52 (1992)
101. G.A. Ragoisha, A.S. Bondarenko, N.P. Osipovich, E.A. Streltsov, Potentiodynamic electrochemical impedance spectroscopy of lead upd on polycrystalline gold and on selenium atomic underlayer. Electrochem. Commun. **7**, 631–636 (2005)
102. L. Beaunier, I. Epelboin, J.C. Lestrade, H. Takenouti, Electrochemical and scanning microscope study of pained Fe. Surf. Technol. **4**, 237 (1976)
103. F. Mansfield, M. Kendig, S. Tsai, Evaluation of corrosion behavior of coated metals with AC impedance measurements. Corrosion **38**(7), 478–485 (1982)
104. A. Ramanavicius, A. Finkelsteinas, H. Cesiulis, A. Ramanaviciene, Electrochemical impedance spectroscopy of polypyrolle based immunosensor. Bioelectrochemistry **79**(1), 11–16 (2010)
105. P.L. Bonora, F. Deflorian, L. Fedrizzi. Electrochemical impedance spectroscopy as a tool for investigating underpaint corrosion. Electrochimica Acta **41**(7–8), 1073–1082 (1996)
106. J. Padgurskas, R. Rukuiza, H. Cesiulis, A. Amulevicius, A. Daugvila, R. Davidonis, C. Sipavicius, The properties and physicochemical interactions in the system iron-fluoroligomer. Physicochem. Mech. Mater. **45**(5), 81–90 (2009)
107. J. Padgurskas, R. Rukuiza, A. Amulevicius, C. Sipavicius, K. Mazeika, R. Davidonis, A. Daugvila, H. Cesiulis, Influence of fluor-oligomers on the structural and tribological properties of steel surface at the rolling friction. Ind. Lubr. Tribol **60**(5), 222–227 (2008)
108. V.F. Lvovich, M.F. Smiechowski, Non-linear impedance analysis of industrial lubricants. Electrochim. Acta **53**(25), 7375–7385 (2008)
109. D. Hallam, D. Thurrowgood, V. Otieno-Alego, D. Creagh, An EIS Method for assessing thin oil films used in museums, in *Proceedings of Metal 2004 National Museum of Australia Canberra ACT*, 4–8 October 2004 ABN 70 592 297 967, pp. 388–399
110. L. Jianguo, G. Gaoping, Y. Chuanwei, EIS study of corrosion behaviour of organic coating/Dacromet composite systems. Electrochimica Acta **50**(16–17), 3320–3332 (2005)
111. Y.J. Tan, S. Balley, B. Kinsella, An investigation of the formation and destruction of corrosion inhibitor films using electrochemical impedance spectroscopy (EIS). Corros. Sci. **38**(9), 1545–1561 (1996)
112. S. González, M.A. Gil, J.O. Hernández, V. Fox, R.M. Souto, Resistance to corrosion of galvanized steel covered with an epoxy-polyamide primer coating. Prog. Org. Coat. **41**, 167–170 (2001)
113. H. Cesiulis, N. Tsyntsaru, Non-destructive method for assessing thin oil films, in *Proceedings of the International Conference BALTTRIB'2009* (2009), pp. 59–64
114. J.J. Santana, J.E. González, J. Morales, S. González, R.M. Souto, Evaluation of ecological organic paint coatings via electrochemical impedance spectroscopy. Int. J. Electrochem. Sci. **7**, 6489–6500 (2012)
115. N. Hammouda, H. Chadli, G. Guillemot, K. Belmokre, The corrosion protection behaviour of zinc rich epoxy paint in 3 % NaCl solution advances in chemical. Eng. Sci. **1**, 51–60 (2011)
116. B.M. Fernández-Pérez, J.A. González-Guzmán, S. González, R.M. Souto, Electrochemical impedance spectroscopy investigation of the corrosion resistance of a waterborne acrylic coating containing active electrochemical pigments for the protection of carbon steel. Int. J. Electrochem. Sci. **9**, 2067–2079 (2014)

117. P.L. Bonora, F. Deflorian, L. Fedrizzi. Electrochemical impedance spectroscopy as a tool for investigating underpaint corrosion. Electrochimica Acta **41**(7–8), 1073–1082 (1996)
118. H. Cesiulis, G. Baltrūnas, J. Padgurskas, The effect of FOLEOX thin films on the corrosion behaviour of Armco iron. Mater. Sci. (Medziagotyra) **8**(4), 392–395 (2002)
119. G.W. Walter, A review of impedance plot methods used for corrosion performance analysis of painted metals. Corros. Sci. **26**(9), 681–703 (1986)
120. Y.J. Tom, S. Bailey, An investigation on the formation and destruction of corrosion inhibitor films using electrochemical noise analysis (ENA). Corros. Sci. **38**(9), 1545–1561 (1996)
121. A. Banu, O, Radovici, M. Marcu, T. Spataru, S. Jurcoane, Electrochemical synthesis and characterization of a polipyrrole/lipase composite film. Roum. Biotechnol. Lett. **13**(1), 3551–3556 (2008)
122. I. Morkvenaite-Vilkonciene, P. Genys, A. Ramanaviciene, A. Ramanavicius, Scanning electrochemical impedance microscopy for investigation of glucose oxidase catalyzed reaction colloids and surfaces. B-Biointerfaces **126**, 598–602 (2015)
123. I. Lapenaite, A. Ramanaviciene, A. Ramanavicius, Current trends in enzymatic determination of glycerol. Crit. Rev. Anal. Chem. **36**, 13–25 (2006)
124. A. Ramanavicius, A. Ramanaviciene, A. Malinauskas, Electrochemical sensors based on conducting polymer—polypyrrole (Review). Electrochim. Acta **51**, 6025–6037 (2006)
125. Y. Oztekin, A. Ramanaviciene, Z. Yazicigil, A.O. Solak, A. Ramanavicius, Direct electron transfer from glucose oxidase immobilized on polyphenanthroline modified-glassy carbon electrode. Biosens. Bioelectron. **26**, 2541–2546 (2011)
126. N. German, A. Ramanaviciene, A. Ramanavicius, Electrochemical deposition of gold nanoparticles on graphite rod for glucose biosensing. Sens. Actuators B: Chem. **203**, 25–34 (2014)
127. A. Ramanavicius, P. Genys, A. Ramanaviciene, Electrochemical impedance spectroscopy based evaluation of 1,10-Phenanthroline-5,6-dione and glucose oxidase modified graphite electrode. Electrochim. Acta **146**, 659–665 (2014)
128. A. Ramanavicius, P. Genys, Y. Oztekin, A. Ramanaviciene, Evaluation of the redox mediating properties of 1,10-Phenanthroline-5,6-dione for glucose oxidase modified graphite electrodes. J. Electrochem. Soc. **161**, B31–B33 (2014)
129. D.D. Macdonald, Reflections on the history of electrochemical impedance spectroscopy. Electrochim. Acta **51**, 1376–1388 (2006)
130. R.K. Shervedani, A.H. Mehrjardi, N. Zamiri, A novel method for glucose determination based on electrochemical impedance spectroscopy using glucose oxidase self-assembled biosensor. Bioelectrochemistry **69**, 201–208 (2006)
131. T. Hoshino, S. Sekiguchi, H. Muguruma, Amperometric biosensor based on multilayer containing carbon nanotube, plasma-polymerized film, electron transfer mediator phenothiazine, and glucose dehydrogenase. Bioelectrochemistry **84**, 1–5 (2012)
132. B. Kurtinaitiene, D. Ambrozaite, V. Laurinavicius, A. Ramanaviciene, A. Ramanavicius, Amperometric immunosensor for diagnosis of BLV infection. Biosens. Bioelectron. **23**, 1547–1554 (2008)
133. Y. Oztekin, A. Ramanaviciene, N. Ryskevic, Z. Yazicigil, Z. Ustundag, A.O. Solak, A. Ramanavicius, 1,10-Phenanthroline modified glassy carbon electrode for voltammetric determination of cadmium(II) ions. Sens. Actuators B: Chem. **157**, 146–153 (2011)
134. Y. Oztekin, Z. Yazicigil, A. Ramanaviciene, A. Ramanavicius, Polyphenol-modified glassy carbon electrodes for copper detection. Sens. Actuators B: Chem. **152**, 37–48 (2011)
135. Y. Oztekin, Z. Yazicigil, A. Ramanaviciene, A. Ramanavicius, Square wave voltammetry based determination of copper (II) ions by polyluteolin- and polykaempferol-modified electrodes. Talanta **85**, 1020–1027 (2011)
136. A. Ramanaviciene, A. Ramanavicius, Pulsed amperometric detection of DNA with an ssDNA/polypyrrole modified electrode. Anal. Bioanal. Chem. **379**, 287–293 (2004)
137. A. Ramanavicius, Y. Oztekin, A. Ramanaviciene Electrochemical Formation of Polypyrrole-based layer for immunosensor design. Sens. Actuators B: Chem. **197**, 237–243 (2014)

138. V. Ratautaite, S.D. Janssens, K. Haenen, M. Nesládek, A. Ramanaviciene, I. Baleviciute, A. Ramanavicius, Molecularly imprinted polypyrrole based impedimentric sensor for theophylline determination. Electrochim. Acta **130**, 361–367 (2014)
139. V. Ratautaite, D. Plausinaitis, I. Baleviciute, L. Mikoliunaite, A. Ramanaviciene, A. Ramanavicius, Characterization of caffeine-imprinted polypyrrole by a quartz crystal microbalance and electrochemical impedance spectroscopy. Sens. Actuators B: Chem. **212**, 63–71 (2015)
140. A. Ramanaviciene, A. Finkelsteinas, A. Ramanavicius, Basic electrochemistry meets nanotechnology: Electrochemical preparation of artificial receptors based on a nanostructured conducting polymer, polypyrrole. J. Chem. Educ. **83**, 1212–1214 (2006)
141. A. Ramanaviciene, A. Ramanavicius, Molecularly imprinted polypyrrole-based synthetic receptor for direct detection of bovine leukemia virus glycoproteins. Biosens. Bioelectron. **20**, 1076–1082 (2004)
142. V. Ratautaite, S.N. Topkaya, L. Mikoliunaite, M. Ozsoz, Y. Oztekin, A. Ramanaviciene, A. Ramanavicius, Molecularly imprinted polypyrrole for DNA determination. Electroanalysis **25**, 1169–1177 (2013)
143. A. Ramanaviciene, A. Ramanavicius, Application of polypyrrole for the creation of immunosensors. Crit. Rev. Anal. Chem. **32**, 245–252 (2002)
144. D. Plausinaitis, V. Ratautaite, L. Mikoliunaite, L. Sinkevicius, A. Ramanaviciene, A. Ramanavicius, Quartz crystal microbalance based evaluation of electrochemical formation of aggregated polypyrrole particle based layer. Langmuir **31**(10), 3186–3193 (2015)
145. A. Ramanaviciene, N. German, A. Kausaite-Minkstimiene, J. Voronovic, J. Kirlyte, A. Ramanavicius, Comparative study of surface plasmon resonance, electrochemical and electroassisted chemiluminescence methods based immunosensor for the determination of antibodies against human growth hormone. Biosens. Bioelectron. **36**, 48–55 (2012)
146. A.S. Bandarenka, K. Eckhard, A. Maljusch, W. Schuhmann, Localized electrochemical impedance spectroscopy: Visualization of spatial distributions of the key parameters describing solid/liquid interfaces. Anal. Chem. **85**, 2443–2448 (2013)
147. V. Kuznetsov, A. Maljusch, R.M. Souto, A.S. Bandarenka, W. Schuhmann, Characterization of localised corrosion processes using scanning electrochemical impedance microscopy. Electrochem. Commun. **44**, 38–41 (2014)
148. L. Philippe, G. Walter, S. Lyon, Investigating localized degradation of organic coatings comparison of electrochemical impedance spectroscopy with local electrochemical impedance spectroscopy. J. Electrochem. Soc. **150**, B111–B119 (2003)
149. K. Darowicki, M. Szociński, A. Zieliński, Assessment of organic coating degradation via local impedance imaging. Electrochim. Acta **55**, 3741–3748 (2010)
150. M. Szociński, K. Darowicki, K. Schaefer, Identification and localization of organic coating degradation onset by impedance imaging. Polym. Degrad. Stab. **95**, 960–964 (2010)
151. A. Ramanavicius, A. Kausaite-Minkstimiene, I. Morkvenaite-Vilkonciene, P. Genys, R. Mikhailova, T. Semashko, J. Voronovic, A. Ramanaviciene, Biofuel cell based on glucose oxidase from Penicillium funiculosum 46.1 and horseradish peroxidase. Chem. Eng. J. **264**, 165–173 (2015)
152. A. Ramanavicius, Y. Oztekin, A. Ramanaviciene, Electrochemical formation of polypyrrole-based layer for immunosensor design. Sens. Actuators B: Chem. **197**, 237–243 (2014)
153. M.V. Mirkin, W. Nogala, J. Velmurugan, Y. Wang, Scanning electrochemical microscopy in the 21st century. Update 1: five years after. Phys. Chem. Chem. Phys. **13**, 21196–21212 (2011)
154. M. Ciobanu, D.E. Taylor, J.P. Wilburn, D.E. Cliffel, Glucose and lactate biosensors for scanning electrochemical microscopy imaging of single live cells. Anal. Chem. **80**, 2717–2727 (2008)
155. D.T. Pierce, P.R. Unwin, A.J. Bard, Scanning electrochemical microscopy. 17. Studies of enzyme-mediator kinetics for membrane- and surface-immobilized glucose oxidase. Anal. Chem. **64**, 1795–1804 (1992)

156. B.R. Horrocks, D. Schmidtke, A. Heller, A.J. Bard, Scanning electrochemical microscopy. 24. Enzyme ultramicroelectrodes for the measurement of hydrogen peroxide at surfaces. Anal. Chem. **65**, 3605–3614 (1993)
157. K. Eckhard, T. Erichsen, M. Stratmann, W. Schuhmann, Frequency-dependent alternating-current scanning electrochemical microscopy (4D AC-SECM) for local visualisation of corrosion sites. Chem. Eur. J. **14**, 3968–3976 (2008)
158. K. Eckhard, C. Kranz, H. Shin, B. Mizaikoff, W. Schuhmann, Frequency dependence of the electrochemical activity contrast in AC-scanning electrochemical microscopy and atomic force microscopy-AC-scanning electrochemical microscopy imaging. Anal. Chem. **79**, 5435–5438 (2007)
159. P.M. Diakowski, Z.F. Ding, Novel strategy for constant-distance imaging using alternating current scanning electrochemical microscopy. Electrochem. Commun. **9**, 2617–2621 (2007)
160. B. Ballesteros, A. Katemann, E.J. Schulte, M. Calvo, W. Koudelka-Hep, Schuhmann, Localised electrochemical impedance spectroscopy with high lateral resolution by means of alternating current scanning electrochemical microscopy. Electrochem. Commun. **4**, 134–138 (2002)
161. C. Gabrielli, M. Keddam, N. Portail, P. Rousseau, H. Takenouti, V. Vivier, Electrochemical impedance spectroscopy investigations of a microelectrode behavior in a thin-layer cell: experimental and theoretical studies. J. Phys. Chem. B **110**, 20478–20485 (2006)
162. C. Gabrielli, F. Huet, M. Keddam, P. Rousseau, V. Vivier, Scanning electrochemical microscopy imaging by means of high-frequency impedance measurements in feedback mode. J. Phys. Chem. B **108**, 11620–11626 (2004)
163. A.S. Baranski, P.M. Diakowski, Application of AC impedance techniques to scanning electrochemical microscopy. J. Solid State Electrochem. **8**, 683–692 (2004)
164. K. Eckhard, H. Shin, B. Mizaikoff, W. Schuhmann, C. Kranz, Alternating current (AC) impedance imaging with combined atomic force scanning electrochemical microscopy (AFM-SECM). Electrochem. Commun. **9**, 1311–1315 (2007)

http://www.springer.com/978-3-319-30197-6

Nanostructures and Thin Films for Multifunctional Applications
Technology, Properties and Devices
Tiginyanu, I.; Topala, P.; Ursaki, V. (Eds.)
2016, XXIV, 576 p. 364 illus., 296 illus. in color.,
Hardcover
ISBN: 978-3-319-30197-6